mathematics

MDPI

Article

Secure Impulsive Control of Singular Markovian Jump Neural Networks Against Hybrid Attacks: A Hybrid Event-Triggered Mechanism

Weiwei Xing and Yijun Zhang *

School of Automation, Nanjing University of Science and Technology, Nanjing 210094, China; xingwwvip@njust.edu.cn

* Correspondence: zhangyijun@njust.edu.cn

Abstract

This paper investigates the hybrid event-triggered impulsive control problem of singular Markovian jump neural networks (SMJNNs). The simultaneous presence of denial-of-service (DoS) attacks and deception attacks (DAs) over the communication network is explicitly addressed. To facilitate a bandwidth-adaptive scheduling framework, a mode-dependent dynamic event-triggered mechanism (DETMα_i^d) is proposed, wherein the dynamic threshold is adaptively adjusted by utilizing both real-time bandwidth occupancy and the Markovian mode. Furthermore, to effectively mitigate the severe data losses caused by DoS attacks, an immediate triggering mechanism (DETMα_i^a) is activated at the attack ending instants. Integrating DETMα_i^a and DETMα_i^d yields a hybrid event-triggered mechanism (HETM), which governs the impulsive instants of the designed mode-dependent impulsive controller. In addition, by systematically analyzing the evolution of the constructed Lyapunov–Krasovskii functional (LKF) over both continuous intervals and impulsive instants, LMI-based sufficient conditions are derived to guarantee the global exponential admissibility of the SMJNNs. Finally, numerical simulations and analog resistance–capacitance (RC) network circuit experiments are conducted to demonstrate the effectiveness of the proposed approach.

Keywords: Markovian jump system; singular neural networks; hybrid event-triggered mechanism; hybrid cyber-attacks; impulsive control

MSC: 34A09; 93B70; 93D05

1. Introduction

Singular systems, which combine dynamic evolution with algebraic constraints, offer a more comprehensive description of practical systems compared to traditional state-space models. Up to now, they have been widely applied in power electronic circuits, aerospace, and chemical processes [1–3]. As a result, singular systems have garnered extensive scholarly investigation. For instance, Ref. [4] addressed the asymptotic stability problem in positive fractional-order singular systems, and Ref. [5] tackled the issue of fault-tolerant optimal control for fractional-order singular systems. Consequently, the application of singular systems within the framework of complex networked control systems (NCSs) merits further in-depth investigation.

Neural networks are characterized as a class of nonlinear systems composed of a multitude of interconnected units. They have attracted sustained interest owing to their

Check for updates

Academic Editor: Sabri Arik

Received: 11 September 2026
Revised: 29 September 2026
Accepted: 1 October 2026
Published: 3 October 2026

Copyright: © 2026 by the authors. Licensee MDPI, Basel, Switzerland. This article is an open access article distributed under the terms and conditions of the Creative Commons Attribution (CC BY) license.

extensive applications in computer vision, autonomous vehicle control and signal processing [6,7]. Over the past decade, significant progress has been made in this field. For instance, Ref. [8] investigated the tracking control problem for adaptive neural networks, and [9] discussed the H_∞ control issue for delayed neural networks. Building on these advancements, the study of singular neural networks has emerged as an important research topic. Ref. [10] investigated the consensus problem of neural networks for singular fractional-order multiagent systems and developed an effective state feedback sliding mode control strategy.

As a specialized category of switched systems, Markovian jump systems are well-suited for modeling practical systems with sudden parametric and structural transitions [11]. Over recent decades, significant progress has been made in the admissibility analysis of singular Markovian jump systems (SMJSs). Specifically, for discrete singular piecewise homogeneous Markovian jump systems, Ref. [12] focused on stability analysis and Ref. [13] addressed the problem of sliding mode control. Additionally, Ref. [14] investigated the asynchronous H_∞ filtering issue for delayed singular Markovian jump neural networks.

Furthermore, the intrinsic openness of communication channels renders NCSs increasingly susceptible to various cyber-attacks, such as DoS attacks and deception attacks (DAs), which can jeopardize stability, degrade the desired control performance, and disrupt communication channels [15]. Considerable research efforts have been dedicated to counteracting the adverse consequences of cyber-attacks within the framework of networked systems. Focusing on the scenario where DAs and DoS attacks occur independently, Ref. [16] developed a resilient control scheme for switched systems. Nevertheless, limited results are available regarding secure control for the SMJNNs affected by stochastic cyber-attacks, which serves as the primary motivation for this study.

To alleviate the communication burden under limited bandwidth, event-triggered mechanisms (ETMs) have been extensively studied. Unlike time-triggered mechanisms, ETMs ensure that data is transmitted only when a specific triggering condition is satisfied [17]. Generally, ETMs can be classified into two fundamental categories: static ETMs (SETMs) and dynamic ETMs (DETMs) [18]. While SETMs are straightforward to implement, they often result in a conservative triggering frequency due to their fixed parameters. To further reduce the communication burden, DETMs have been developed to provide more flexible triggering laws, which significantly reduce redundant transmissions without sacrificing desired control performance [19]. Recently, DETMs have been increasingly adopted in SMJSs to optimize the utilization of limited network resources. For instance, a dynamic-memory event-triggered transmission strategy (DMETS) was proposed for asynchronous control of singular stochastic semi-Markov jump systems [20]. However, this mechanism remains inflexible as it fails to account for the stochasticity and complexity of network bandwidth occupancy, which underscores the necessity for further designs of bandwidth-adaptive ETMs.

Due to its critical significance in stability analysis and synchronization for linear or nonlinear systems, impulsive control has attracted a great deal of attention in the control field. Ref. [21] introduced dynamic event-triggered impulsive control to achieve uniform stability for inertial delayed neural networks. Moreover, the authors designed a delayed secure impulsive law and resolved the issue of secure impulsive synchronization for dynamic networks [22]. Despite recent developments, the issue of impulsive control for SMJNNs remains insufficiently investigated, thereby motivating the present research.

It is worth noting that although advanced control methods, such as state filtered disturbance rejection control [23] and multilayer neuroadaptive reinforcement learning [24], have exhibited remarkable superiority in handling complex disturbances and unknown dynamics, they often rely on continuous state measurements or struggle to directly address

hard algebraic constraints. Consequently, in the face of communication interruptions induced by intermittent DoS attacks and the inherent algebraic structure of singular systems, the direct application of these methods is significantly restricted. This further motivates our study to explore a hybrid event-triggered impulsive secure control scheme for SMJNNs subject to DoS attacks and DAs. This study addresses three primary challenges: (1) establishing a generalized mathematical framework that comprehensively characterizes singular constraints, Markovian jumps and external complex network threats; (2) monitoring the network bandwidth occupancy and designing appropriate ETMs by taking both the limited bandwidth and desired transmission performance into consideration; (3) developing an analysis method to guarantee the exponential admissibility of SMJNNs. To address these challenges, the primary contributions of this work are summarized as follows.

- A unified secure control framework for SMJNNs is developed. Different from the single-type cyber-attacks studied in [25,26], this framework simultaneously addresses inherent algebraic constraints, time-delayed nonlinear neuron activation functions, and hybrid cyber-threats. Furthermore, a mode-dependent impulsive controller is designed to mitigate the adverse effects of DoS attacks and DAs on the SMJNNs.
- A novel HETM is proposed to enable bandwidth-adaptive communication scheduling, which encompasses two distinct triggering rules to handle different network scenarios. Unlike existing passive or fixed-threshold mechanisms [15,20,27], the proposed HETM dynamically adapts to the actual cyber-attack status to actively counteract DoS jamming. Specifically, the $DETM\alpha_i^a$ is activated at the end instant of the DoS attack to recover the system from communication disruptions induced by DoS attacks; the $DETM\alpha_i^d$ is activated during the sleep window of the DoS attack to adapt to the network bandwidth status dynamically and schedule data transmissions selectively. Ultimately, the proposed HETM achieves a trade-off between communication resource conservation and secure control.
- A comprehensive co-design criterion is established. By overcoming the difficulties induced by nonlinearities, singular matrices, time delays, and Markovian jumps, sufficient conditions are derived. This method not only guarantees the exponential admissibility of the SMJNNs but also enables the co-design of the impulsive controller and the event-triggered mechanism.

Notations: Throughout this paper, $\mathbb{R}$, $\mathbb{R}^n$, $\mathbb{R}^{n\times m}$ and $\mathbb{D}_+^n$ denote the set of real numbers, the n-dimensional Euclidean space, the set of $n \times m$ real matrices and the set of diagonal matrices with n positive elements, respectively. $E^\dagger$ denotes the Moore–Penrose pseudoinverse of matrix E. The set of positive integers is represented by $\mathbb{N}$, while $\mathbb{N}_0 = \mathbb{N} \cup \{0\}$ denotes the set of non-negative integers. The superscript T stands for matrix transposition. $\mathrm{Sym}\{Q\}$ denotes $Q + Q^T$. $\mathrm{rank}(Q)$ denotes the rank of the matrix Q. The symbol $*$ in $\begin{bmatrix} Q_1 & Q_2 \\ * & Q_3 \end{bmatrix}$ represents the symmetric block induced by Q_2. $\lambda_{\max}(\cdot)$ and $\lambda_{\min}(\cdot)$ denote the maximum and minimum eigenvalues of the relevant matrix, respectively. $\mathbb{E}\{\cdot\}$ and $\|\cdot\|$ signify the expectation operator and Euclidean norm, respectively. $\mathrm{Prob}\{\cdot\}$ is the probability measure.

2. Model Formulation and Preliminaries

2.1. System Description

Consider the following SMJNNs

$$\begin{cases} E\dot{x}(t) = A(r_t)x(t) + G_1(r_t)g(x(t)) + G_2(r_t)g(x(t-d(t)) + B(r_t)u(t) \\ y(t) = C(r_t)x(t) \end{cases} \tag{1}$$

where $x(t) \in \mathbb{R}^n$, $u(t) \in \mathbb{R}^m$ and $y(t) \in \mathbb{R}^q$ denote the internal state vector, the control input and the measured output, respectively. $g(x(t)) = [g(x_1(t)), g(x_2(t)), \cdots, g(x_n(t))]^T$ represents the neuron activation function satisfying Lemma 1. $d(t)$ is the time-varying delay, which is a differentiable function satisfying $0 \leq d(t) \leq \bar{d}$ and $\dot{d}(t) \leq \mu_d < 1$. The matrices $A(r_t)$, $G_1(r_t)$, $G_2(r_t)$, $B(r_t)$ and $C(r_t)$ are mode-dependent system matrices with appropriate dimensions. The matrix $E \in \mathbb{R}^{n\times n}$ is a singular matrix that satisfies $\text{rank}(E) = r < n$. Furthermore, the overall framework is depicted in Figure 1.

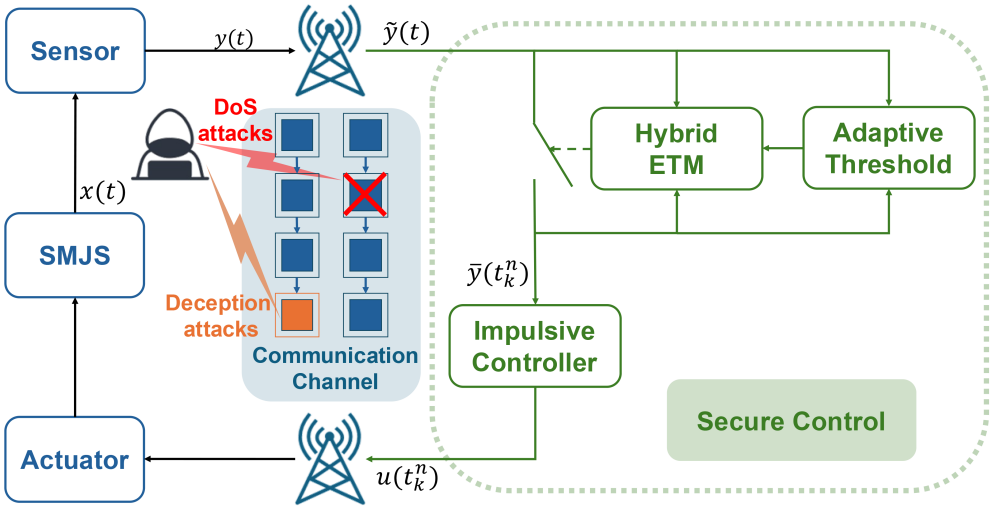


Figure 1. The framework of the SMJNNs with the hybrid ETM subject to DoS attacks and DAs.

Remark 1. *It is worth noting that the assumption $\dot{d}(t) \leq \mu_d < 1$ is a standard theoretical requirement in delay-dependent stability analysis [14,28]. While it is theoretically possible to relax this bound by adopting delay-independent methods, such approaches inevitably inject significant conservatism into the stability criteria, often rendering the LMI conditions infeasible for complex singular systems. Given the inherent algebraic constraints of singular systems, adopting the delay-dependent method with a bounded derivative is essential to derive practically feasible sufficient conditions while minimizing analytical conservatism.*

Lemma 1 ([29])**.** *Let $h(x(s))$ be the neuron activation function. For any positive definite diagonal matrices $\mathcal{D} \in \mathbb{D}_+^n$, the following quadratic inequality holds for all $s \in \mathbb{R}^n$.*

$$0 \leq [\underline{K}_m x(s) - h(x(s))]^T \mathcal{D}[h(x(s)) - \overline{K}_m x(s)]$$

where the diagonal gain matrices are defined as $\underline{K}_m = \text{diag}\{k_1^-, k_2^-, \cdots, k_n^-\}$ and $\overline{K}_m = \text{diag}\{k_1^+, k_2^+, \cdots, k_n^+\}$.

The system parameter variations are governed by a continuous-time Markov process $\{r_t, t \geq 0\}$ taking values in a finite set $\mathcal{N} = \{1, 2, \cdots, N\}$, and the transition rate matrix $\Pi = [\pi_{ij}]$, $i, j \in \mathcal{N}$ conforms to the common conditions [30,31]. For notational simplicity, when the mode $r_t = i$, we denote the associated system matrices as A_i, B_i, C_i, G_{1i} and G_{2i}.

Remark 2. *Over the past decade, singular systems have attracted a surge in research interest, yielding fruitful results on SMJSs [32,33] and singular systems under deception attacks [34] or singular systems under DoS attacks [25]. However, despite these significant advancements, there is limited literature concerning SMJNNs against hybrid cyber-attacks, which more accurately capture concurrent threats in open networks. To bridge this gap, the developed model (1) presents a hybrid system framework by taking Markov jump parameters, hybrid cyber-attacks, and time-delayed neural networks into account simultaneously, which is different from existing works. Particularly,*

the adopted hybrid attack model aims to more accurately capture concurrent threats in practical networks. While this comprehensive model inevitably increases the analytical complexity, it provides a more realistic foundation for the subsequent secure control design.

2.2. Hybrid Cyber-Attacks

It is well-established that data transmission over communication channels is susceptible to malicious cyber-attacks, which pose severe threats to system stability and control performance. This part specifically addresses the impact of deception attacks, whose occurrence is modeled as a stochastic process governed by a Bernoulli-distributed variable $\beta(t)$. Consequently, the measurement output, potentially compromised by the adversary as depicted in Figure 1, is denoted by $\bar{y}(t)$ and described as follows:

$$\bar{y}(t) = \beta(t)y(t) + \tilde{\beta}(t)f(y(t)). \tag{2}$$

with $\tilde{\beta}(t) = 1 - \beta(t)$.

Remark 3. *In practical engineering scenarios, although the exact mathematical form of the attack function $f(y(t))$ is unknown, its magnitude is inevitably restricted by the attacker's finite power capabilities, network bandwidth limits, and the physical saturation of sensors. Consequently, it is both reasonable and practically significant to assume that $f(y(t))$ satisfies the sector-bounded constraint outlined in Lemma 1 [22,26]. In the formulated attack model (2), the stochastic variable $\beta(t)$ accounts for the random occurrence of the DAs, reflecting the unreliability of the open communication channel. Specifically, the expectation and variance are described as $Prob\{\beta(t) = 1\} = \bar{\beta}$, $Prob\{\tilde{\beta}(t)\} = \bar{\tilde{\beta}} = 1 - \bar{\beta}$, and $Var\{\beta(t)\} = \mathbb{E}\{(\beta(t) - \bar{\beta})^2\} = \bar{\beta}\bar{\tilde{\beta}}$. These statistical characteristics are essential for analyzing the mean-square stability of the SMJNNs under consideration.*

Beyond the risks of DAs, the reliability of the control system is further challenged by DoS attacks. While DAs may tamper with the data packets, DoS attacks aim to sever the sensor-to-controller link entirely. To capture the physical constraints of such attacks, we assume the DoS jamming occurs in an aperiodic and intermittent fashion with reference to Figure 2.

$$\tilde{y}(t) = \mathscr{D}_D(t)\bar{y}(t), \tag{3}$$

with

$$\mathscr{D}_D(t) = \begin{cases} 1, & t \in [s_n, s_n + \ell_n), \\ 0, & t \in [s_n + \ell_n, s_{n+1}). \end{cases} \tag{4}$$

Let s_n and ℓ_n represent the initiation instant and the duration of the $(n+1)$-th recovery phase with $n \in \mathbb{N}_0$, respectively. Based on these two parameters, the time axis is partitioned into two distinct intervals: the communication window $\mathcal{I}_{\text{on},n} \triangleq [s_n, s_n + \ell_n)$ and the attack window $\mathcal{I}_{\text{off},n} \triangleq [s_n + \ell_n, s_{n+1})$.

It is pertinent to mention that sustaining a continuous DoS jamming is usually impractical in real-world NCSs [27,35]. Motivated by this fact, we introduce starting instants s_n and durations ℓ_n to characterize the intermittent attack behavior. Specifically, the open-loop operation induced by DoS attacks is mitigated gradually during the recovery intervals $\mathcal{I}_{\text{on},n}$, where the re-established network channel facilitates the recovery of system performance. To mathematically characterize the properties of the DoS attack, the occurrence frequency and duration of DoS attacks are assumed as follows.

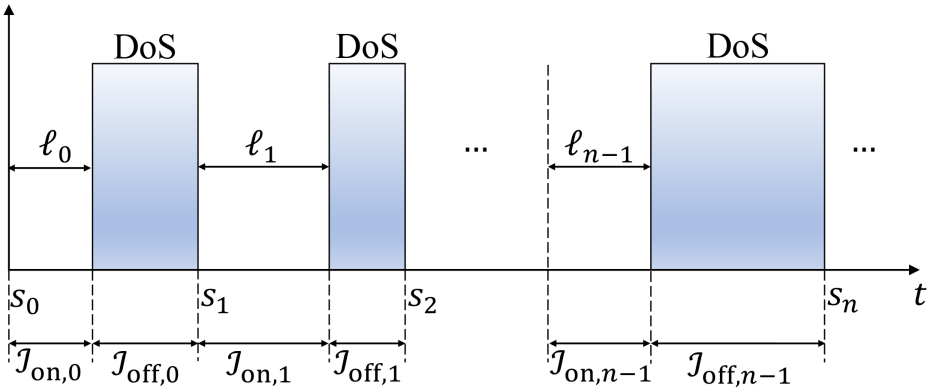


Figure 2. The diagram of aperiodic DoS jamming attacks.

Assumption 1 ([35]). *Let $\mathcal{C}(s,t)$ signify the total number of DoS attacks occurring during the interval $[s,t)$. For pre-specified constants $\nu \geq 0$ and $\tau_D > 0$, the frequency of the DoS attacks is required to adhere to*

$$\mathcal{C}(s,t) \leq \nu + \frac{t-s}{\tau_D}$$

Assumption 2 ([35]). *The duration of the transmission-on intervals $\mathcal{I}_{\text{on},n}$ and transmission-off intervals $\mathcal{I}_{\text{off},n}$ are bounded by*

$$\mathbb{T}_{\min} \leq \inf_{n\in\mathbb{N}}\{\ell_n\}, \quad \mathbb{T}_{\max} \geq \sup_{n\in\mathbb{N}}\{s_{n+1}-s_n-\ell_n\}$$

where $\mathbb{T}_{\min} > 0$ represents the minimum guaranteed communication time, and $\mathbb{T}_{\max} \geq 0$ is the maximum allowable jamming duration.

2.3. Mode-Dependent HETM Under Hybrid Attacks

To maximize transmission efficiency and maintain system performance within the limited communication windows, this part proposes a mode-dependent hybrid event-triggered mechanism (HETM).

Before proceeding to the formal analysis, it is essential to define the fundamental variables. Within this HETM framework, let h signify the sampling period, thus the discrete-time sampling instants are represented by the sequence $\mathcal{S} \triangleq \{mh \mid m \in \mathbb{N}_0\}$. Under the constraints of the proposed HETM and the intermittent DoS jamming environment, only a fraction of these data packets can reach the controller successfully. We define the sequence of successful transmission instants as $\mathcal{T} \triangleq \{t_k^n \mid t_k^n \in \mathcal{I}_{\text{on},n}, n \in \mathbb{N}_0, k = 0,1,\cdots,N_n\}$, where t_k^n represents the $(k+1)$-th successful transmission instant occurring within the $(n+1)$-th communication window $\mathcal{I}_{\text{on},n}$, and N_n denotes the index of the last successful transmission during $\mathcal{I}_{\text{on},n}$. Furthermore, the transmission sequence $\mathcal{T}$ constitutes a subsequence of $\mathcal{S}$, satisfying $t_0^0 < t_1^0 < \cdots < t_{N_n}^n < t_0^{n+1} < \cdots$, with $\lim_{n\to\infty} t_{N_n}^n = \infty$. More specifically, the next event-triggering instant is governed according to the following execution rule:

$$\begin{cases} t_0^n = \inf\{t = mh \mid t \geq s_n\}, \\ t_{k+1}^n = \inf\{t = mh > t_k^n \mid \hat{\mu}_i \pi(mh) \geq \chi_i(mh),\ t \in (s_n, s_n + \ell_n)\}. \end{cases} \tag{5}$$

Here, mh denotes the current sampling instant. Accordingly, we define $\pi(mh) = e_k^T(mh)\Omega_i e_k(mh) - \sigma_i(mh)\bar{y}^T(t_k^n)\Omega_i\bar{y}(t_k^n)$, $e_k(mh) = \bar{y}(t_k^n) - \bar{y}(mh)$ for $m = 0,\cdots,\bar{m}$ with $\bar{m} \triangleq \sup\{m \in \mathbb{N}_0 \mid mh < t_{k+1}^n\}$. Moreover, $\sigma_i(mh) \in (0,1)$ is the triggering parameter, $\hat{\mu}_i$ is a positive scalar to be given, and $\Omega_i > 0$ represents the mode-dependent weighting

matrix to be designed for the i-th subsystem, $i \in \mathcal{N}$. Furthermore, Figure 3 illustrates the sequence of data transmission through HETM (5) subjected to hybrid cyber-attacks.

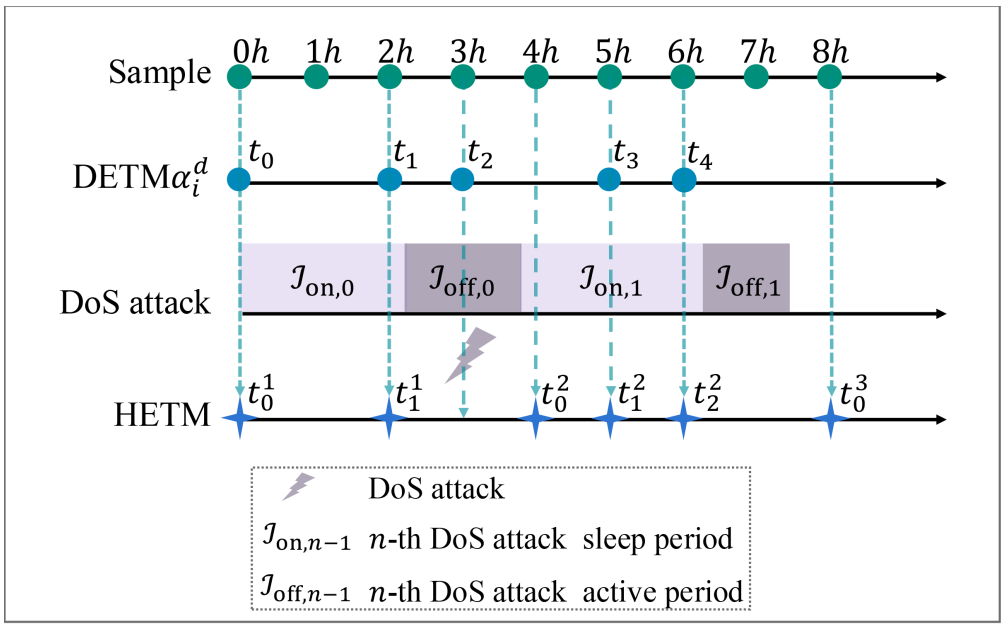


Figure 3. The triggering sequence of Hybrid ETM (5) exposed to DoS attacks.

Remark 4. *The HETM in (5) adopts a dual-mode mechanism to balance system security and communication efficiency. More specifically,*

- *DETMα_i^a: Compared to the passive defense strategy in [20], which lacks an immediate post-attack compensatory mechanism, the DETMα_i^a counteracts DoS jamming by enforcing a state update at the first available sampling instant upon network recovery, denoted as t_0^n. This action swiftly bridges the state information gap to accelerate system convergence. Furthermore, by eliminating excessive error accumulation, it averts the onset of intensive triggering in the subsequent DETMα_i^d, ensuring the robustness and secure control for SMJNNs (1).*
- *DETMα_i^d: In contrast to the event-triggered impulsive control frameworks in [15,27], which predominantly rely on fixed thresholds or adaptive laws without considering the real-time network burden, the DETMα_i^d employs a dynamic threshold $\sigma_i(mh)$ with the weighting parameter α_i that evolves according to system state errors and real-time bandwidth status. It focuses on resource optimization by filtering out redundant data packets when the system state is within no DoS attack region, ensuring an efficient utilization of limited bandwidth.*

The variable $\chi_i(mh)$ in (5) is an auxiliary dynamic variable governed by

$$\begin{cases} \dot{\chi}_i(t) = -\lambda_i \chi_i(t) - \hat{\kappa}_i \pi(t), & t = mh \in (t_k^n, t_{k+1}^n) \\ \chi_i(t_{k+1}^n) = \psi_i \chi_i(t_{k+1}^n)^-, & t = t_{k+1}^n \end{cases} \tag{6}$$

where $\lambda_i > 0$, $\hat{\kappa}_i > 0$ and $\psi_i \geq 1$ are mode-dependent constants assigned to the i-th subsystem with the initial condition $\chi_i(0) = \chi_{i0} > 0$, $i \in \mathcal{N}$.

Remark 5. *Inspired by the DETM in [36], the auxiliary variable $\chi_i(mh)$ in (6) is composed of two dynamic parts: a continuous evolution equation for intervals (t_k^n, t_{k+1}^n), and a discrete reset occurring at the triggering instants t_{k+1}^n. The continuous part can adaptively regulate the dynamic variable based on the system's real-time state. Meanwhile, the discrete part utilizes the parameter ψ_i to instantaneously reset the variable value upon triggering, ensuring synchronization with the impulsive control updates of the SMJNNs (1). It is worth noting that, compared to the globally fixed*

reset parameters utilized in [36], the HETM introduces mode-dependent design parameters like $\lambda_i, \hat{\kappa}_i, \psi_i$ to dynamically adjust according to the stochastic Markovian modes, which can provide a more flexible and customized trade-off between communication resource conservation and system security under intermittent DoS attacks.

Moreover, the dynamic threshold parameter $\sigma_i(mh)$ is formulated by the following equation with the mode-dependent weighting factor $\alpha_i \in [0,1]$.

$$\sigma_i(mh) = \alpha_i \rho_i(mh) + (1-\alpha_i)\hbar_i(mh) \tag{7}$$

Remark 6. *For the SMJNNs (1), the mode-dependent α_i allows for flexible adjustment in view of the real-time network bandwidth and transmission requirements. This individualized control strategy ensures the overall system maintains robust performance and achieves secure control even during frequent mode transitions and intermittent DoS attacks.*

To facilitate the trigger design, several positive scalars ϵ_{1i}, ϵ_{2i} and $\underline{\sigma}_i, \bar{\sigma}_i \in [0,1)$ are introduced for each mode $i \in \mathcal{N}$. The initial conditions for two dynamic variables $\rho_i(mh)$ and $\hbar_i(mh)$ are constrained by $0 \le \rho_i(0) \le \underline{\sigma}_i \le \hbar_i(0) \le \bar{\sigma}_i$ with $\underline{\sigma}_i \in [0, \bar{\sigma}_i)$. For notation brevity, let the sampling instants mh and $(m+1)h$ be denoted by m and $m+1$, respectively. Under this convention, the recursive evolution of $\rho_i(m)$ and $\hbar_i(m)$ is determined by

$$\begin{cases} \rho_i(m+1) = \frac{\rho_i(m)}{1+\epsilon_{1i}\rho_i(m)e_k^T(m)\Omega_i e_k(m)} \\ \hbar_i(m+1) = \frac{\hbar_i(m)e_k^T(m)\Omega_i e_k(m)+\epsilon_{2i}\bar{\sigma}_i}{\epsilon_{2i}+e_k^T(m)\Omega_i e_k(m)} \end{cases} \tag{8}$$

Remark 7. *It is noteworthy that the update laws in (8) are formulated to preserve the positive definiteness and boundedness of the threshold variables $\sigma_i(m)$. Provided that the initial conditions satisfy the inequality $0 \le \rho_i(0) \le \underline{\sigma}_i \le \hbar_i(0) \le \bar{\sigma}_i$, it can be established that $\rho_i(m) \in [0, \underline{\sigma}_i)$ and $\hbar_i(m) \in [\underline{\sigma}_i, \bar{\sigma}_i]$ for all $m \in \mathbb{N}_0$. This property is fundamental in ensuring the feasibility of the LMI-based stability conditions.*

Remark 8. *The dynamic triggering threshold $\sigma_i(m)$ in (7) is constructed as a convex combination of $\rho_i(m)$ and $\hbar_i(m)$ in (8), modulated by the weighting parameter $\alpha_i \in [0,1]$. Specifically, $\rho_i(m)$ ensures high-frequency data transmission to counteract attack-induced adverse effects during the sleep window with the monotonically nonincreasing property, and $\hbar_i(m)$ is responsible for maintaining high-quality data transmission by reducing the triggering frequency with the monotonically nondecreasing property. The design parameters ϵ_{1i} and ϵ_{2i} allow for a customized trade-off between communication efficiency and control performance for each Markov mode $i \in \mathcal{N}$. Taken together, the design of threshold $\sigma_i(m)$ incorporates the requirements for optimizing network resource utilization and guaranteeing control performance.*

To facilitate the stability analysis of the SMJNNs (1), we decompose the sleep window into two intervals: the transmission interval $R_k^n = [t_k^n, t_{k+1}^n)$ with $k = 0, 1, \cdots, N_n$ and the final truncated interval $R_{k(n)}^n$. Note that $\mathcal{I}_{\text{on},n} = \left(\bigcup_{k=0}^{N_n-1} R_k^n\right) \cup R_{k(n)}^n$ for $n \in \mathbb{N}_0$. Thus, a piecewise function is adopted for simplicity following the approach [37].

$$\tau_k(t) = \begin{cases} t - t_k^n, & t \in [t_k^n, t_k^n + h) \\ t - t_k^n - h, & t \in [t_k^n + h, t_k^n + 2h) \\ \vdots & \\ t - t_k^n - \bar{m}h, & t \in [t_k^n + \bar{m}h, t_{k+1}^n) \end{cases} \tag{9}$$

Consequently, the error term $e_k(t)$ is defined as

$$e_k(t) = \begin{cases} 0, & t \in [t_k^n, t_k^n + h) \\ \bar{y}(t_k^n) - \bar{y}(t_k^n + h), & t \in [t_k^n + h, t_k^n + 2h) \\ \vdots & \\ \bar{y}(t_k^n) - \bar{y}(t_k^n + \bar{m}h), & t \in [t_k^n + \bar{m}h, t_{k+1}^n) \end{cases} \tag{10}$$

Accordingly, it is readily observed that $\tau_k(t) \in [0, h)$ when $t \in \mathcal{I}_{\text{on},n}$. Based on this, we can get the following formula $\bar{y}(t_k^n) = \bar{y}(t - \tau_k(t)) + e_k(t)$.

2.4. Impulsive Controller

Predicated on the sequence of triggering instants, the impulsive controller subjected to deception and DoS attacks is constructed as

$$u(t) = K_i \tilde{y}(t)\delta(t - t_k^n) = K_i \bar{y}(t)\delta(t - t_k^n) \tag{11}$$

where $\delta(\cdot)$ represents the Dirac impulse function active exclusively at the triggering instants t_k^n. The set of impulsive instants synchronizes strictly with the signal transmission sequence generated by the HETM in (5). The matrix $K_i \in \mathbb{R}^{m\times m}$ represents the Markov-dependent impulsive controller gain to be determined.

Combining (1) and (11) yields the following closed-loop impulsive system.

$$\begin{cases} E\dot{x}(t) = A_i x(t) + G_{1i} g(x(t)) + G_{2i} g(x(t - d(t))) & t \in \mathcal{I}_{\text{off},n} \\ E\dot{x}(t) = A_i x(t) + G_{1i} g(x(t)) + G_{2i} g(x(t - d(t))) & t \in \mathcal{I}_{\text{on},n}, t \neq t_k^n \\ x((t_k^n)^+) = x((t_k^n)^-) + B_i K_i \bar{y}((t_k^n)^-) & t \in \mathcal{I}_{\text{on},n}, t = t_k^n \\ x(t) = \phi(t), & t \in [-h, 0] \end{cases} \tag{12}$$

where $\phi(t)$ denotes the initial function of $x(t)$.

To facilitate the derivation of the main results, the following necessary definitions and auxiliary lemmas are presented.

Lemma 2. *Given the positive scalars $\lambda_i, \hat{\kappa}_i, \hat{\mu}_i$ and χ_{i0}, it follows that the auxiliary dynamic variable $\chi_i(t) \geq 0$ for all $t \in [0, \infty)$.*

Proof. Firstly, for any $t \in (t_k^n, t_{k+1}^n)$, substituting $\chi_i(t) > \hat{\mu}_i \pi(t)$ derived from (5) into (6) yields

$$\dot{\chi}_i(t) = -\lambda_i \chi_i(t) - \hat{\kappa}_i \pi(t) > -\left(\lambda_i + \frac{\hat{\kappa}_i}{\hat{\mu}_i}\right)\chi_i(t),$$

Thus, the inequality $\chi_i(t) \geq \chi_{i0} \mathrm{e}^{-\left(\lambda_i + \frac{\hat{\kappa}_i}{\hat{\mu}_i}\right)t} \geq 0$ is satisfied for any $t \in [0, \infty)$ except the triggering instants $t = t_k^n$.

Subsequently, at the triggering instants $t = t_k^n$, it can be derived from (6) that

$$\chi_i(t_k^n) = \psi_i \chi_i((t_k^n)^-),$$

Given $\psi_i \geq 1$ and $\chi_i((t_k^n)^-) \geq 0$, it directly follows that $\chi_i(t_k^n) \geq 0$.

Consequently, we conclude that $\chi_i(t) \geq 0$ holds for $t \in [0, \infty)$ based on $\chi_{i0} > 0$. □

Lemma 3 ([38]). *Let H be a symmetric matrix and $H = \begin{bmatrix} H_1 & H_2 \\ * & H_3 \end{bmatrix}$, where H_1 and H_3 are square matrices. Then, the inequality $H < 0$ holds if and only if*

$$H_3 < 0, \quad H_1 - H_2 H_3^{-1} H_2^T < 0,$$

Alternatively, this is equivalent to

$$H_1 < 0, \quad H_3 - H_2^T H_1^{-1} H_2 < 0.$$

Lemma 4 ([39]). *Consider the symmetric matrices $\Phi_i \in \mathbb{R}^{n\times n}$ $(i = 0, 1, \cdots, p)$ and a vector variable $\eta \in \mathbb{R}^n$. The following deduction*

$$\eta^T \Phi_1 \eta \geq 0, \cdots, \eta^T \Phi_p \eta \geq 0 \implies \eta^T \Phi_0 \eta < 0,$$

is valid provided that there exist scalars $\lambda_1, \cdots, \lambda_p \geq 0$ such that

$$\Phi_0 + \lambda_1 \Phi_1 + \cdots + \lambda_p \Phi_p < 0.$$

Definition 1 ([28]). *The continuous-time SMJNNs described in (12) are characterized as follows:*

- ***Regular and Impulse-free:*** *The SMJNNs are deemed regular and impulse-free provided that the matrix pair (E, A_i) is regular and impulse-free for any mode $i \in \mathcal{N}$;*
- ***Exponentially Stable:*** *The SMJNNs achieve exponential stability in the mean square sense if there exist positive scalars κ and λ such that the state trajectory satisfies $\mathbb{E}\{\|x(t)\|^2\} \leq \kappa e^{-\lambda t}\mathbb{E}\{\|x(0)\|^2\}$ for any initial state $x(0)$;*
- ***Exponentially Admissible:*** *If the SMJNNs simultaneously satisfy the conditions of regularity, impulse freeness and exponential stability, it is termed exponentially admissible.*

3. Main Results

To facilitate the subsequent stability analysis, we refine the effective DoS attack intervals and define the associated variables.

First, a continuous DoS attack is effective if and only if it blocks the sampled data. Therefore, the continuous attack window $\mathcal{I}_{\text{off},n}$ is equivalently redefined as an effective DoS window $\bar{\mathcal{I}}_{\text{off},n} \triangleq [t_m^n, t_p^n)$, where $t_m^n = \min\{kh \in \mathcal{S} \mid kh \geq s_n + \ell_n\}$ and $t_p^n = \min\{kh \in \mathcal{S} \mid kh \geq s_{n+1}\}$. Consequently, the effective communication window becomes $\bar{\mathcal{I}}_{\text{on},n} \triangleq [t_p^{n-1}, t_m^n)$.

Furthermore, for notational brevity, let $x_{k,n}(t) = x(t - \tau_k(t))$ and $f_k(t) = f(y(t - \tau_k(t)))$. The augmented vector is partitioned into $\xi(t) = [\xi_1^T(t), \xi_2^T(t), \xi_3^T(t)]^T$ with

$$\begin{aligned}
\xi_1(t) =& \text{col}\{x(t), g(x(t)), g(x(t - d(t)))\}, \\
\xi_2(t) =& \text{col}\{x(t - d(t)), x(t - h), x(t - \bar{d})\}, \\
\xi_3(t) =& \text{col}\{x_{k,n}(t), f_k(t), e_k(t)\}.
\end{aligned}$$

Accordingly, the associated matrices are defined as $\mathcal{F}_\ell = [\mathcal{F}_{\ell,1}, \mathcal{F}_{\ell,2}, \mathcal{F}_{\ell,3}]$ and

$$\mathcal{M}_i = [\mathcal{M}_{i,1}, \underbrace{0, \ldots, 0}_{6 \text{ blocks}}], \quad \text{with} \quad \mathcal{M}_{i,1} = [A_i, G_{1i}, G_{2i}].$$

Theorem 1. *Under Assumptions 1 and 2, the SMJNN in (12) is exponentially admissible subject to hybrid cyber-attacks for any mode $r_t = i \in \mathcal{N}$, if, for bounded scalars $\bar{\beta} \in [0, 1]$, $\rho_i(0) \leq \underline{\sigma}_i \leq \hbar_i(0) \leq \bar{\sigma}_i$, $\varpi_1 > 1$, $\varpi_2 > 1$, $\psi_i \geq 1$, positive scalars $N_{\max}$, τ_D, $\mathbb{T}_{\min}$, $\mathbb{T}_{\max}$, γ_1, γ_2, λ_i, $\hat{\kappa}_i$, $\hat{\mu}_i$, χ_{i0}, ϵ_{1i}, ϵ_{2i}, τ_{imp}, ϑ_i, μ_i, ν, and prescribed diagonal matrices $\underline{L}_1$, $\bar{L}_1$, $\underline{L}_2$, $\bar{L}_2$, $\underline{L}_3$, $\bar{L}_3$,*

there exist symmetric positive-definite matrices $P_{1i}, P_{2i}, Q_{1j}, Q_{2j}$ $(j = 1, 2, 3)$, Ω_i, Q_{imp}, *positive diagonal matrices* $\Lambda_1, \Lambda_2, \Lambda_3$, *and appropriately dimensioned matrices* $R, N_i, \mathcal{F}_1, \mathcal{F}_2$, *such that the following LMIs are feasible for* $\ell \in \{1, 2\}$.

$$\Sigma^{\ell i} = \begin{bmatrix} \Xi_{11}^{\ell i} + \text{Sym}(\mathcal{F}_{\ell,1}^T R^T \mathcal{M}_{i,1}) & \Xi_{12}^{\ell i} + \mathcal{M}_{i,1}^T R \mathcal{F}_{\ell,2} & \mathcal{M}_{i,1}^T R \mathcal{F}_{\ell,3} \\ * & \Xi_{22}^{\ell i} & 0 \\ * & * & \Xi_{33}^{\ell i} \end{bmatrix} < 0, \tag{13}$$

$$P_{1i} \le \varpi_2 P_{2i}, \quad P_{2i} \le \varpi_1 \gamma_0 P_{1i}, \quad Q_{1j} \le \varpi_2 Q_{2j}, \quad Q_{2j} \le \varpi_1 Q_{1j}, \quad j = 1, 2, 3, \tag{14}$$

$$\begin{bmatrix} -\vartheta_i \hat{Z}_i - 2\tau_{\text{imp}} C_i^T \underline{L}_1^T \Lambda_1 \bar{L}_1 C_i & \tau_{\text{imp}} C_i^T (\underline{L}_1^T + \bar{L}_1^T) \Lambda_1 & -(I + \bar{\beta} M_i)^T \\ * & -2\tau_{\text{imp}} \Lambda_1 & -(1 - \bar{\beta}) N_i^T \\ * & * & -Q_{\text{imp}} \end{bmatrix} < 0, \tag{15}$$

$$\begin{bmatrix} \hat{Z}_i & I \\ I & Q_{\text{imp}} \end{bmatrix} > 0, \quad (I - EE^{\dagger}) N_i = 0, \tag{16}$$

$$\varpi_1 \varpi_2 \mu_{\max}^{N_{\max}} \mathrm{e}^{2(\gamma_1+\gamma_2)h - 2\gamma_1 \mathbb{T}_{\min} + 2\gamma_2 \mathbb{T}_{\max}} < 1, \tag{17}$$

where

$$\Xi_{11}^{\ell i} = \begin{bmatrix} \tilde{\Xi}_{11}^{\ell i} & E^T P_{\ell i} G_{1i} + (\underline{L}_2 + \bar{L}_2)^T \Lambda_2 & E^T P_{\ell i} G_{2i} \\ * & -2\Lambda_2 & 0 \\ * & * & -2\Lambda_3 \end{bmatrix},$$

$$\Xi_{22}^{\ell i} = \text{diag}\{ -(1 - \mu_d) c_{\bar{d}}^{\ell} Q_{\ell 1} - 2\underline{L}_3^T \Lambda_3 \bar{L}_3, \ -c_h^{\ell} Q_{\ell 2}, \ -c_{\bar{d}}^{\ell} Q_{\ell 3} \},$$

$$\Xi_{33}^{\ell i} = \begin{bmatrix} -2C^T \underline{L}_1^T \Lambda_1 \bar{L}_1 C - \tilde{\mathcal{K}}_{\ell i} \sigma_i^* \bar{\beta} C^T \Omega_i C & C^T (\underline{L}_1 + \bar{L}_1)^T \Lambda_1 & -\tilde{\mathcal{K}}_{\ell i} \sigma_i^* \bar{\beta} C^T \Omega_i \\ * & -2\Lambda_1 & \tilde{\mathcal{K}}_{\ell i} \sigma_i^* \bar{\beta} \Omega_i \\ * & * & \tilde{\mathcal{K}}_{\ell i} (1 - \sigma_i^*) \Omega_i \end{bmatrix},$$

$$\Xi_{12}^{\ell i} = \begin{bmatrix} 0 & 0 & 0 \\ 0 & 0 & 0 \\ (\underline{L}_3 + \bar{L}_3)^T \Lambda_3 & 0 & 0 \end{bmatrix},$$

with $\tilde{\Xi}_{11}^{\ell i} = \text{Sym}(E^T P_{\ell i} A_i) + (-1)^{\ell - 1} 2\gamma_{\ell} E^T P_{\ell i} E + \sum_{j=1}^{N} \pi_{ij} E^T P_{\ell j} E + \sum_{m=1}^{3} Q_{\ell m} - 2\underline{L}_2^T \Lambda_2 \bar{L}_2$.

The related parameters are definedas $\tilde{\beta} = 1 - \bar{\beta}$, $\mu_i = \max(\vartheta_i, 1, \psi_i)$, $\mu_{\max} = \max\{\mu_i\}$, $c_h^{\ell} = \mathrm{e}^{(-1)^{\ell} 2\gamma_{\ell} h}$, $c_{\bar{d}}^{\ell} = \mathrm{e}^{(-1)^{\ell} 2\gamma_{\ell} \bar{d}}$, $\gamma_0 = \mathrm{e}^{2(\gamma_1+\gamma_2)h}$, $Z_i = E^T P_{1i} E$, $\hat{Z}_i = Z_i + \epsilon I$, $M_i = N_i C_i$, $\tilde{\mathcal{K}}_{\ell i} = (2\gamma_{\ell} - \lambda_i)\hat{\mu}_i - \hat{\kappa}_i$, *and* $R \in \mathbb{R}^{n \times (n-r)}$ *is any full-column rank matrix satisfying* $E^T R = 0$. *In this case, assuming* B_i *has full column rank, the designed Markovian-dependent impulsive controller gains can be given by*

$$K_i = (B_i^T B_i)^{-1} B_i^T N_i$$

Proof. First, we investigate the regularity and impulse freeness of the system. According to LMI condition (13) with $\ell = 1$, $Q \triangleq \sum_{m=1}^{3} Q_{1m}$, we can derive

$$\begin{bmatrix} \tilde{\Xi}_{11}^{\ell i} & E^T P_{1i} G_{1i} + (\underline{L}_2^T + \bar{L}_2^T) \Lambda_2 \\ * & -2\Lambda_2 \end{bmatrix} < 0 \tag{18}$$

with $\tilde{\Xi}_{11}^{1i} = \text{Sym}(E^T P_{1i} A_i + F_{1,1}^T R^T A_i) + 2\gamma_1 E^T P_{1i} E + \sum_{j=1}^{N} \pi_{ij} E^T P_{1j} E + Q - 2\underline{L}_2^T \Lambda_2 \bar{L}_2$.

Suppose that $A_{22,i}$ is singular. Then, there exists a non-zero vector $v \in \mathbb{R}^{n-r}$ such that $A_{22,i}v = 0$. Since $\text{rank}(E) = r < n$, there exist non-singular matrices $X_1, X_2 \in \mathbb{R}^{n\times n}$ satisfying $X_1 E X_2 = \text{diag}\{I_r, 0\}$. Correspondingly, we derive

$$R = X_1^T[0, \mathbb{R}_2^T]^T, \;\; X_2^T F_{1,1}^T = [\check{F}_{1,1}, \bar{F}_{1,1}]^T.$$

where $\mathbb{R}_2 \in \mathbb{R}^{(n-r)\times(n-r)}$ is an arbitrary non-singular matrix, and $\check{F}_{1,1} \in \mathbb{R}^{(n-r)\times r}$, $\bar{F}_{1,1} \in \mathbb{R}^{(n-r)\times(n-r)}$ are partitioned matrices with appropriate dimensions.

Define $\eta = [0_{1\times r}, v^T]^T \in \mathbb{R}^n$. Pre- and post-multiplying (18) by $\text{diag}\{\eta^T X_2^T, I\}$ and $\text{diag}\{X_2\eta, I\}$ yields

$$\eta^T X_2^T E^T = \eta^T \text{diag}\{I_r, 0\} X_1^{-T} = 0$$

and

$$\eta^T X_2^T F_{1,1}^T R^T A_i X_2 \eta = [0, v^T] \begin{bmatrix} \check{F}_{1,1}^T \\ \bar{F}_{1,1}^T \end{bmatrix} [0, \mathbb{R}_2] X_1 A_i X_2 \begin{bmatrix} 0 \\ v \end{bmatrix} = v^T \bar{F}_{1,1}^T \mathbb{R}_2 A_{22,i} v = 0$$

and

$$\begin{bmatrix} \eta^T X_2^T \left(Q - 2\underline{L}_2^T \Lambda_2 \bar{L}_2\right) X_2\eta & \eta^T X_2^T (\underline{L}_2^T + \bar{L}_2^T)\Lambda_2 \\ * & -2\Lambda_2 \end{bmatrix} < 0$$

By applying the Schur complement (Lemma 3) to the above inequality, we obtain

$$\eta^T X_2^T \Big[(Q - 2\underline{L}_2^T \Lambda_2 \bar{L}_2) - (\underline{L}_2^T + \bar{L}_2^T)\Lambda_2(-2\Lambda_2)^{-1}\Lambda_2(\underline{L}_2 + \bar{L}_2) \Big] X_2\eta < 0$$

The above inequality can be equivalently rewritten as

$$\eta^T X_2^T \left[Q + \frac{1}{2}(\bar{L}_2 - \underline{L}_2)^T \Lambda_2 (\bar{L}_2 - \underline{L}_2) \right] X_2\eta < 0 \tag{19}$$

Notice that $Q > 0, \Lambda_2 > 0$ and $(\bar{L}_2 - \underline{L}_2)^T \Lambda_2 (\bar{L}_2 - \underline{L}_2) \geq 0$, which implies

$$\eta^T X_2^T \left[Q + \frac{1}{2}(\bar{L}_2 - \underline{L}_2)^T \Lambda_2 (\bar{L}_2 - \underline{L}_2) \right] X_2\eta > 0$$

which contradicts (19).

Consequently, $A_{22,i}$ must be non-singular, confirming that the system (12) is regular and impulse-free. Furthermore, the non-singularity of $A_{22,i}$ inherently guarantees that the algebraic variables of the singular system are uniquely determined by the differential variables. Therefore, the consistency conditions for the initial states are naturally satisfied without requiring direct algebraic decoupling based on singular value decomposition as often seen in existing work [32].

Subsequently, in order to prove the exponential stability of the SMJNNs (12), the following mode-dependent LKF is considered to address two cases under DoS attacks.

- When the effective communication window is active, $t \in \bar{\mathcal{I}}_{\text{on},n} \setminus \{t_k^n\}$,

$$V_1(x_t, i, t) = \sum_{j=1}^{3} V_{1j}(x_t, i, t) \tag{20}$$

- When the effective DoS window is active, $t \in \bar{\mathcal{I}}_{\text{off},n}$,

$$V_2(x_t, i, t) = \sum_{j=1}^{3} V_{2j}(x_t, i, t) \tag{21}$$

with

$$V_{\ell 1}(x_t, i, t) = x^T(t)E^T P_{\ell i} E x(t) \tag{22}$$

$$V_{\ell 2}(x_t, t) = \int_{t-d(t)}^{t} \mathrm{e}_\ell(s) x^T(s) Q_{\ell 1} x(s) \mathrm{d}s + \int_{t-h}^{t} \mathrm{e}_\ell(s) x^T(s) Q_{\ell 2} x(s) \mathrm{d}s + \int_{t-\bar{d}}^{t} \mathrm{e}_\ell(s) x^T(s) Q_{\ell 3} x(s) \mathrm{d}s \tag{23}$$

$$V_{\ell 3}(x_t, t) = \chi_i(t) \tag{24}$$

where $\ell \in \{1, 2\}$, and $\mathrm{e}_\ell(s) = \mathrm{e}^{2\cdot(-1)^\ell \gamma_\ell (t-s)}$. Here, $\chi_i(t)$ is the auxiliary dynamic variable defined in (6), which is integrated into the LKF to facilitate the co-design of the DETM. In particular, $\ell = 1$ applies to the effective communication window $t \in \bar{\mathcal{I}}_{\mathrm{on},n} \setminus \{t_k^n\}$, whereas $\ell = 2$ corresponds to the effective DoS attack window $t \in \bar{\mathcal{I}}_{\mathrm{off},n}$.

Denoted by $\mathcal{L}$ the weak infinitesimal operator is associated with the stochastic process $\{x(t), r_t, t \geq 0\}$. For any given mode $r_t = i \in \mathcal{N}$, the operator $\mathcal{L}$ acting on the LKF $V(x_t, i, t)$ is defined using the following limit:

$$\mathcal{L}V(x_t, i, t) = \lim_{\Delta \to 0^+} \frac{1}{\Delta} [\mathbb{E}\{V(x_{t+\Delta}, r_{t+\Delta}, t+\Delta) \mid x_t, r_t = i\} - V(x_t, i, t)]$$

Firstly, we consider the DoS sleep window with $\ell = 1$, and we obtain

$$\begin{aligned} \mathcal{L}V_{11}(x_t, i, t) =& -2\gamma_1 V_{11}(x_t, i, t) + 2\gamma_1 x^T(t) E^T P_{1i} E x(t) \\ &+ x^T(t) \left(\sum_{j=1}^{N} \pi_{ij} E^T P_{1j} E \right) x(t) \\ &+ 2x^T(t) E^T P_{1i} [A_i x(t) + G_{1i} g(x(t)) + G_{2i} g(x(t - d(t)))] \end{aligned} \tag{25}$$

Exploiting the delay condition $0 \leq d(t) \leq \bar{d}$, $\dot{d}(t) \leq \mu_d < 1$ and denoting $c_h^1 = \mathrm{e}^{-2\gamma_1 h}$ and $c_{\bar{d}}^1 = \mathrm{e}^{-2\gamma_1 \bar{d}}$, we have

$$\begin{aligned} \mathcal{L}V_{12}(x_t, t) \leq& -2\gamma_1 V_{12}(x_t, t) + x^T(t)(Q_{11} + Q_{12} + Q_{13}) x(t) \\ &- (1 - \mu_d) c_{\bar{d}}^1 x^T(t - d(t)) Q_{11} x(t - d(t)) \\ &- c_h^1 x^T(t - h) Q_{12} x(t - h) - c_{\bar{d}}^1 x^T(t - \bar{d}) Q_{13} x(t - \bar{d}) \end{aligned} \tag{26}$$

Furthermore, according to mechanism (7) and updating laws (8), the time-varying parameter satisfies $\sigma_i(t) \leq \alpha_i \underline{\sigma}_i + (1 - \alpha_i)\bar{\sigma}_i \triangleq \sigma_i^*$. Taking the derivative of $V_{13}(x_t, t)$ during the interval $t \in (t_k^n, t_{k+1}^n)$ yields

$$\begin{aligned} \mathcal{L}V_{13}(x_t, t) =& -2\gamma_1 V_{13}(x_t, t) + 2\gamma_1 V_{13}(x_t, t) + \dot{\chi}_i(t) \\ \leq& -2\gamma_1 V_{13}(x_t, t) + \tilde{\mathcal{K}}_{1i} \times (e_k^T(t) \Omega_i e_k(t) - \sigma_i(t) [\beta(t) x_{k,n}^T(t) C^T \\ &+ \tilde{\beta}(t) f_k^T(t) + e_k^T(t)] \Omega_i [\beta(t) C x_{k,n}(t) + \tilde{\beta}(t) f_k(t) + e_k(t)]) \\ \leq& -2\gamma_1 V_{13}(x_t, t) + \tilde{\mathcal{K}}_{1i} \times (e_k^T(t) \Omega_i e_k(t) - \sigma_i^* [\beta(t) x_{k,n}^T(t) C^T \\ &+ \tilde{\beta}(t) f_k^T(t) + e_k^T(t)] \Omega_i [\beta(t) C x_{k,n}(t) + \tilde{\beta}(t) f_k(t) + e_k(t)]) \end{aligned} \tag{27}$$

with $\tilde{\beta}(t) = 1 - \beta(t)$, $\tilde{\mathcal{K}}_{1i} = (2\gamma_1 - \lambda_i)\hat{\mu}_i - \hat{\kappa}_i$.

According to Lemma 1, we have

$$\begin{aligned} &2(f_k(t) - \underline{L}_1 C x_{k,n}(t))^T \Lambda_1 (\bar{L}_1 C x_{k,n}(t) - f_k(t)) \geq 0 \\ &2(g(x(t)) - \underline{L}_2 x(t))^T \Lambda_2 (\bar{L}_2 x(t) - g(x(t))) \geq 0 \end{aligned}$$

$$2(g(x(t-d(t))) - \underline{L}_3 x(t-d(t)))^T \Lambda_3 (\overline{L}_3 x(t-d(t)) - g(x(t-d(t)))) \geq 0 \tag{28}$$

where $\Lambda_j = \text{diag}\{\lambda_{j,1}, \lambda_{j,2}, \cdots, \lambda_{j,m}\} > 0$, $j = 1,2,3$. Also, $\underline{L}_1$, $\overline{L}_1$, $\underline{L}_2$, $\overline{L}_2$, $\underline{L}_3$ and $\overline{L}_3$ are known diagonal matrices.

To provide extra degrees of freedom, the free-weighting matrix $\mathcal{F}_1 = [\mathcal{F}_{1,1}, \mathcal{F}_{1,2}, \mathcal{F}_{1,3}]$ is introduced. From (12), the following zero-equality holds for any matrix R satisfying $E^T R = 0$.

$$\begin{aligned} 0 =& 2\xi^T(t)\mathcal{F}_1^T R^T E\dot{x}(t) \\ =& 2\xi^T(t)\mathcal{F}_1^T R^T \left[A_i x(t) + G_{1i} g(x(t)) + G_{2i} g(x(t-d(t)))\right] \end{aligned} \tag{29}$$

Combining (25)–(29), it follows that

$$\mathcal{L}V_1(x_t, i, t) \leq -2\gamma_1 V_1(x_t, i, t) + \xi^T(t)\Sigma^{1i}\xi(t) \tag{30}$$

where Σ^{1i} is defined in (13).

At the impulsive instants t_k^n, we obtain

$$\begin{aligned} \mathbb{E}\{V_{11}(t_k^n)\} =& \mathbb{E}\{x^T(t_k^n)E^T P_{1i} E x(t_k^n)\} \\ \leq& \vartheta_i \mathbb{E}\{V_{11}((t_k^n)^-)\} \end{aligned} \tag{31}$$

where $\vartheta_i \in (0,1), i \in \mathcal{N}$ is the related impulsive parameter of $V_{11}(t_k^n)$. The detailed derivation of this impulsive condition (31) is provided in Appendix A.

For LKF (23), we have

$$\mathbb{E}\{V_{12}(t_k^n)\} = \mathbb{E}\{V_{12}((t_k^n)^-)\} \tag{32}$$

Based on the definition of (6), the impulsive jump of V_{13} at t_k^n is governed by the parameter $\psi_i \geq 1$, yielding

$$\mathbb{E}\{V_{13}(t_k^n)\} = \psi_i \mathbb{E}\{V_{13}((t_k^n)^-)\} \tag{33}$$

Combining (31)–(33) yields

$$\begin{aligned} \mathbb{E}\{V_1(t_k^n)\} =& \mathbb{E}\{V_{11}(t_k^n) + V_{12}(t_k^n) + V_{13}(t_k^n)\} \\ \leq& \vartheta_i \mathbb{E}\{V_{11}((t_k^n)^-)\} + \mathbb{E}\{V_{12}((t_k^n)^-)\} + \psi_i \mathbb{E}\{V_{13}((t_k^n)^-)\} \\ \leq& \mu_i \mathbb{E}\{V_1((t_k^n)^-)\} \end{aligned} \tag{34}$$

where the unified impulsive gain μ_i is defined as

$$\mu_i = \max(\vartheta_i, 1, \psi_i), i \in \mathcal{N}. \tag{35}$$

Similarly, during the DoS active window with $\ell = 2$, we have

$$\mathcal{L}V_2(x_t, i, t) \leq 2\gamma_2 V_2(x_t, i, t) + \xi^T(t)\Sigma^{2i}\xi(t) \tag{36}$$

Since $\Sigma^{1i} < 0$ and $\Sigma^{2i} < 0$ in (13), it follows from (30), (34) and (36) that

$$\mathcal{L}V_1(x_t, i, t) + 2\gamma_1 V_1(x_t, i, t) \leq 0, \quad t \in \bar{\mathcal{I}}_{\text{on},n} \setminus \{t_k^n\} \tag{37}$$

$$\mathbb{E}\{V_1(t_k^n)\} \leq \mu_{\max} \mathbb{E}\{V_1((t_k^n)^-)\}, \quad t = t_k^n \tag{38}$$

$$\mathcal{L}V_2(x_t, i, t) - 2\gamma_2 V_2(x_t, i, t) \leq 0, \quad t \in \bar{\mathcal{I}}_{\text{off},n} \tag{39}$$

with $\mu_{\max} = \max\{\mu_i\}$, $i \in \mathcal{N}$.

For the $(n+1)$-th communication window $\bar{\mathcal{I}}_{\text{on},n} = [t_p^{n-1}, t_m^n)$, let $t_0^n < t_1^n < \cdots < t_{N_n}^n < t_m^n$ denote the sequence of impulsive instants with $t_0^n = t_p^{n-1}$. Here, $N_n \le N_{\max}$ is the actual number of triggers, and $N_{\max}$ is the allowable maximum triggers per window.

For the first interval $t \in [t_0^n, t_1^n)$, integrating (37) yields

$$\mathbb{E}\{V_1((t_1^n)^-)\} \le \mathrm{e}^{-2\gamma_1(t_1^n - t_0^n)}\mathbb{E}\{V_1((t_0^n)^+)\} \tag{40}$$

At the first impulsive instant t_1^n, it follows from (38) and (40) that

$$\mathbb{E}\{V_1((t_1^n)^+)\} \le \mu_{\max}\mathrm{e}^{-2\gamma_1(t_1^n - t_0^n)}\mathbb{E}\{V_1((t_0^n)^+)\} \tag{41}$$

Consequently, at the k-th impulsive instant t_k^n, we obtain

$$\mathbb{E}\{V_1(t_k^n)\} \le \mu_{\max}^k\mathrm{e}^{-2\gamma_1(t_k^n - t_0^n)}\mathbb{E}\{V_1((t_0^n)^+)\} \tag{42}$$

Since $k \le N_n \le N_{\max}$ and $\mu_{\max} \ge 1$, it follows from (42) that at the end of the communication window $t = (t_m^n)^-$, the following holds for $t_m^n - t_p^{n-1} \ge \mathbb{T}_{\min}$.

$$\mathbb{E}\{V_1((t_m^n)^-)\} \le \mu_{\max}^{N_{\max}}\mathrm{e}^{-2\gamma_1\mathbb{T}_{\min}}\mathbb{E}\{V_1((t_p^{n-1})^+)\} \tag{43}$$

During the effective attack window $\bar{\mathcal{I}}_{\text{off},n}$, Assumption 2 implies $L_n = t_p^n - t_m^n \le \mathbb{T}_{\max}$. Thus, at the end of this window $t = (t_p^n)^-$, we obtain

$$\mathbb{E}\{V_2((t_p^n)^-)\} \le \mathrm{e}^{2\gamma_2\mathbb{T}_{\max}}\mathbb{E}\{V_2((t_m^n)^+)\} \tag{44}$$

At the switching instants between communication and attack windows, it follows from (14) that

$$\begin{cases} \mathbb{E}\{V_1((t_p^{n-1})^+)\} \le \varpi_2\mathbb{E}\{V_2((t_p^{n-1})^-)\} \\ \mathbb{E}\{V_2((t_m^n)^+)\} \le \varpi_1\mathrm{e}^{2(\gamma_1+\gamma_2)h}\mathbb{E}\{V_1((t_m^n)^-)\} \end{cases} \tag{45}$$

Combining (43)–(45), we derive the following inequality for a complete cycle $[t_p^{n-1}, t_p^n)$.

$$\begin{aligned} \mathbb{E}\{V_1((t_p^n)^+)\} \le & \varpi_2\mathbb{E}\{V_2((t_p^n)^-)\} \\ \le & \varpi_2\mathrm{e}^{2\gamma_2\mathbb{T}_{\max}}\mathbb{E}\{V_2((t_m^n)^+)\} \\ \le & \varpi_2\mathrm{e}^{2\gamma_2\mathbb{T}_{\max}} \times \varpi_1\mathrm{e}^{2(\gamma_1+\gamma_2)h}\mathbb{E}\{V_1((t_m^n)^-)\} \\ \le & \varpi_2\mathrm{e}^{2\gamma_2\mathbb{T}_{\max}} \times \varpi_1\mathrm{e}^{2(\gamma_1+\gamma_2)h} \times \mu_{\max}^{N_{\max}}\mathrm{e}^{-2\gamma_1\mathbb{T}_{\min}}\mathbb{E}\{V_1((t_p^{n-1})^+)\} \\ \le & \aleph\mathbb{E}\{V_1((t_p^{n-1})^+)\}. \end{aligned} \tag{46}$$

with $\aleph \triangleq \varpi_1\varpi_2\mu_{\max}^{N_{\max}}\mathrm{e}^{2(\gamma_1+\gamma_2)h - 2\gamma_1\mathbb{T}_{\min} + 2\gamma_2\mathbb{T}_{\max}}$ defined in (17).

By recursively applying (46) from the initial instant $t = 0$, we obtain

$$\mathbb{E}\{V_1((t_p^{n(t)-1})^+)\} \le \aleph^{n(t)}\mathbb{E}\{V_1(0^+)\}, \quad n(t) \in \mathbb{N}_0. \tag{47}$$

To evaluate the continuous-time dynamics for any $t \ge 0$, suppose $t \in [t_p^{n(t)-1}, t_p^{n(t)})$. When t falls within the communication window $\bar{\mathcal{I}}_{\text{on},n(t)}$, combining (43) and (47) yields

$$\begin{aligned} \mathbb{E}\{V(t)\} \le & \mu_{\max}^{N_{\max}}\mathbb{E}\{V_1((t_p^{n(t)-1})^+)\} \\ \le & \mu_{\max}^{N_{\max}}\aleph^{n(t)}\mathbb{E}\{V_1(0^+)\} \end{aligned} \tag{48}$$

Conversely, when $t \in \bar{\mathcal{I}}_{\text{off},n(t)}$, combining (46) and (47) yields

$$\begin{aligned}\mathbb{E}\{V(t)\} \leq & e^{2\gamma_2 \mathbb{T}_{\max}} \mathbb{E}\{V_2((t_m^{n(t)})^+)\} \\ \leq & \frac{\aleph}{\varpi_2} \mathbb{E}\{V_1((t_p^{n(t)-1})^+)\} \\ \leq & \aleph^{n(t)+1} \mathbb{E}\{V_1(0^+)\} \\ \leq & \aleph^{n(t)} \mathbb{E}\{V_1(0^+)\} \end{aligned} \tag{49}$$

with $\varpi_2 > 1$, $\aleph < 1$ and $\aleph^{n(t)+1} < \aleph^{n(t)} < 1$.

Therefore, by defining $\mathcal{M} \triangleq \max\{\mu_{\max}^{N_{\max}}, 1\}$, it follows from (48) and (49) that for all $t \geq 0$,

$$\mathbb{E}\{V(t)\} \leq \mathcal{M} \aleph^{n(t)} \mathbb{E}\{V_1(0^+)\} \tag{50}$$

Substituting $n(t) \geq t/\tau_D - 1$ into (50) yields

$$\mathbb{E}\{V(t)\} \leq \frac{\mathcal{M}}{\aleph} \aleph^{\frac{t}{\tau_D}} \mathbb{E}\{V_1(0^+)\} = \tilde{\mathcal{M}} e^{-\alpha t} \mathbb{E}\{V(0^+)\} \tag{51}$$

where $\tau_D > 0$ is defined in Assumption 1, $\tilde{\mathcal{M}} = \mathcal{M}/\aleph > 0$ and the decay rate $\alpha = -\frac{\ln \aleph}{\tau_D} > 0$.

According to the inequality (51), the SMJNN (12) is exponentially stable in the mean square sense. Consequently, combining this with the previously proven regularity and impulse freeness, the system is globally exponentially admissible based on Definition 1. □

Remark 9. *Conditions (31), (33) and (35) characterize the energy jump behaviors of the Lyapunov functional V_1 at impulsive instants. Specifically, the constraint on V_{11} in (31) dissipates energy to compensate for delays and cyber-attacks; the condition $\psi_i \geq 1$ in (33) relaxes the event-triggered threshold to conserve network bandwidth; and (35) imposes a strict upper bound μ_i on the overall jump of $V_1(t_k^n)$. Consequently, this mode-dependent coordination facilitates the stability proof and reduces conservatism in the design.*

Remark 10. *Provided that a feasible solution to Theorem 1 exists, the proposed HETM naturally excludes Zeno behavior. Since the triggering logic is evaluated exclusively at periodic sampling instants, the inter-event interval strictly satisfies $t_{k+1}^n - t_k^n \geq h$, thereby precluding an infinite number of triggers within any finite time span.*

4. Numerical Examples

To verify the effectiveness of the proposed control strategy, two examples are provided in this section: a numerical simulation and an analog RC network circuit.

4.1. Example 1

For $i \in \{1, 2, 3\}$, we consider the SMJNN in (1) with the following parameters:

$$A_1 = -\begin{bmatrix} 2.25 & 0 & 0 \\ 0 & 2.1 & 0 \\ 0 & 0 & 1.85 \end{bmatrix}, B_1 = \begin{bmatrix} -0.3 & 0.1 & 0.1 \\ 0.2 & -0.3 & 0.2 \\ 0.2 & 0.1 & -0.3 \end{bmatrix}, C_1 = \begin{bmatrix} -0.01 & -0.2 & 0.1 \\ 0.1 & 0.3 & 0.2 \\ -0.2 & 0.4 & 0.1 \end{bmatrix},$$

$$G_{11} = \begin{bmatrix} 0.5 & 0.5 & 1.5 \\ 0.5 & -1.5 & 1.0 \\ 1.5 & -0.5 & 1.0 \end{bmatrix}, G_{21} = \begin{bmatrix} -1.0 & 0.5 & 1.0 \\ -0.5 & 1.5 & -1.0 \\ 0.5 & -0.5 & 0.5 \end{bmatrix}, \begin{array}{l} \underline{L}_1 = \text{diag}\{0.1, 0.1, 0.05\}, \\ \overline{L}_1 = \text{diag}\{0.8, 0.4, 0.4\}, \end{array}$$

$$A_2 = -\begin{bmatrix} 2.05 & 0 & 0 \\ 0 & 1.75 & 0 \\ 0 & 0 & 1.7 \end{bmatrix}, B_2 = \begin{bmatrix} -0.1 & 0.5 & 0.1 \\ 0.2 & 0.1 & 0.2 \\ 0.2 & 0.4 & -0.1 \end{bmatrix}, C_2 = \begin{bmatrix} -0.1 & 0.1 & 0.1 \\ -0.2 & 0.1 & 0.2 \\ 0.1 & 0.4 & 0.1 \end{bmatrix},$$

$$G_{12} = \begin{bmatrix} -1.0 & 0.5 & 1.5 \\ 1.0 & -2.0 & 1.0 \\ 0.5 & 1.0 & 0.5 \end{bmatrix}, G_{22} = \begin{bmatrix} 2.0 & -1.0 & 1.5 \\ -1.0 & 1.5 & -0.1 \\ 1.5 & -1.5 & 1.0 \end{bmatrix}, \underline{L}_2 = \mathrm{diag}\{0.1, 0.1, 0.1\}, \overline{L}_2 = \mathrm{diag}\{0.75, 0.5, 0.5\},$$

$$A_3 = -\begin{bmatrix} 2.15 & 0 & 0 \\ 0 & 2.2 & 0 \\ 0 & 0 & 2.7 \end{bmatrix}, B_3 = \begin{bmatrix} -0.1 & 0.1 & 0.3 \\ 0.2 & -0.1 & 0.2 \\ 0.2 & 0.2 & 0.1 \end{bmatrix}, C_3 = \begin{bmatrix} -0.1 & 0.2 & -0.1 \\ 0.2 & 0.3 & 0.2 \\ 0.2 & 0.5 & 0.3 \end{bmatrix},$$

$$G_{13} = \begin{bmatrix} -1.5 & 0.5 & -1.0 \\ -0.5 & 1.0 & 2.0 \\ 1.0 & 1.0 & -1.5 \end{bmatrix}, G_{23} = \begin{bmatrix} -1.5 & -0.5 & 1.0 \\ -1.0 & 0.15 & -1.0 \\ 0.15 & -0.5 & 1.0 \end{bmatrix}, \underline{L}_3 = \mathrm{diag}\{0.1, 0.1, 0.1\}, \overline{L}_3 = \mathrm{diag}\{0.75, 0.5, 0.5\},$$

$$E = \begin{bmatrix} 1 & 0 & 0 \\ 0 & 1 & 0 \\ 0 & 0 & 0 \end{bmatrix}, \Pi = \begin{bmatrix} -1.4 & 0.6 & 0.8 \\ 0.3 & -0.7 & 0.4 \\ 0.7 & 0.8 & -1.5 \end{bmatrix}.$$

With a sampling period of $h = 0.1$ s, the HETM parameters for $i = 1, 2, 3$ are configured as: $\bar{\sigma}_i \in \{0.3, 0.6, 0.9\}$, $\underline{\sigma}_i \in \{0.01, 0.3, 0.6\}$, $\alpha_i \in \{0.9, 0.5, 0.2\}$, $\hat{\mu}_i = 1$, $\lambda_i = 0.1$, $\hat{\kappa}_i = 3$, $\psi_i \in \{1.0, 1.05, 1.1\}$, $\epsilon_{1i} = 0.5$, $\epsilon_{2i} = 0.3$, $\chi_{i0} = 0.0001$, $\gamma_1 = 0.5$, $\gamma_2 = 0.4$, $\varpi_1 = \varpi_2 = 1.01$. Moreover, $\bar{d} = 1.5$, $\mu = 0.3$, $\bar{\beta} = 0.45$, $\mathbb{T}_{\min} = 0.7$ and $\mathbb{T}_{\max} = 2$ to simulate a severe cyber threat scenario.

The activation functions are given by $g(x_i(t)) = [0.1x_1(t) + 0.65\tanh(2x_1(t)), 0.1x_2(t) + 0.4\tanh(2x_2(t)), 0.1x_3(t) + 0.4\tanh(2x_3(t))]^T$. The deception attack signal is defined as $f(y(t)) = [0.1y_1(t) + 0.7\tanh(y_1(t)),\ 0.1y_2(t) + 0.3\tanh(y_2(t)), 0.05y_3(t) + 0.35\tanh(y_3(t))]^T$.

By solving LMIs (13)–(17) in Theorem 1, the impulsive controller gains K_i and the corresponding weighting matrices Ω_i are obtained as follows:

$$K_1 = \begin{bmatrix} -1.7706 & 26.2613 & 0.7364 \\ -3.5368 & 41.7178 & 5.0390 \\ -0.9134 & 33.2307 & 2.8158 \end{bmatrix}, \ \Omega_1 = \begin{bmatrix} 0.3776 & 0.1725 & 0.0208 \\ 0.1725 & 0.5293 & -0.2859 \\ 0.0208 & -0.2859 & 0.2740 \end{bmatrix};$$

$$K_2 = \begin{bmatrix} -1.7374 & -2.6984 & -1.7499 \\ 0.2362 & 0.3329 & -0.3814 \\ 0.3584 & 1.5358 & -3.0116 \end{bmatrix}, \ \Omega_2 = \begin{bmatrix} 0.2126 & -0.1183 & -0.0267 \\ -0.1183 & 0.0898 & 0.0054 \\ -0.0267 & 0.0054 & 0.0181 \end{bmatrix};$$

$$K_3 = \begin{bmatrix} -1.0764 & -0.6965 & -2.0105 \\ 3.1776 & -0.1685 & 0.3607 \\ -0.1594 & -1.5480 & -1.7376 \end{bmatrix}, \ \Omega_3 = \begin{bmatrix} 0.0066 & 0.0061 & -0.0055 \\ 0.0061 & 0.0357 & -0.0253 \\ -0.0055 & -0.0253 & 0.0172 \end{bmatrix}.$$

To verify the effectiveness of the impulsive controller (11), the initial condition is set to $x(0) = [2, -1.1, 1]^T$. As shown in Figure 4, the state trajectories asymptotically converge to the equilibrium.

To model varying network traffic, we consider three operational modes governed by the Markov chain r_t: idle with $\alpha_i = 0.9$, moderate with $\alpha_i = 0.5$, and congested with $\alpha_i = 0.2$. Figure 5 illustrates that the adaptive threshold $\sigma_i(t)$ adjusts synchronously with these modes. Specifically, $\sigma_i(t)$ decreases during idle periods, such as $t \in [2.2, 3.1]$ s, to permit more frequent triggering, thereby ensuring system stability. Conversely, it increases under congested conditions to restrict transmissions and alleviate network load.

Furthermore, the DETM α_i^a forces immediate data transmission upon the cessation of a DoS attack to facilitate rapid state recovery. Overall, the proposed HETM successfully co-optimizes communication efficiency and security.

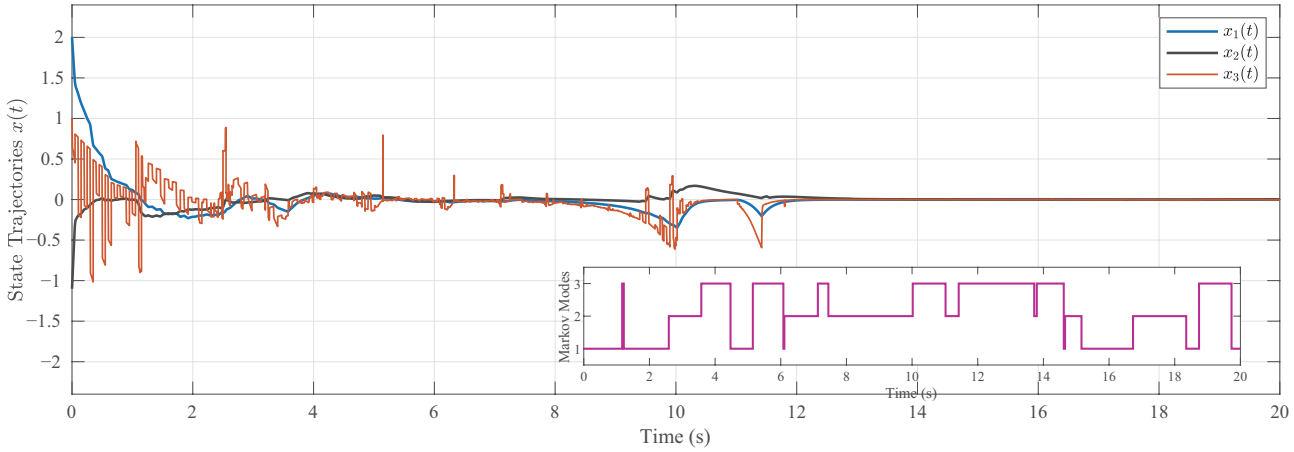


Figure 4. State responses of the SMJNN in Example 1.

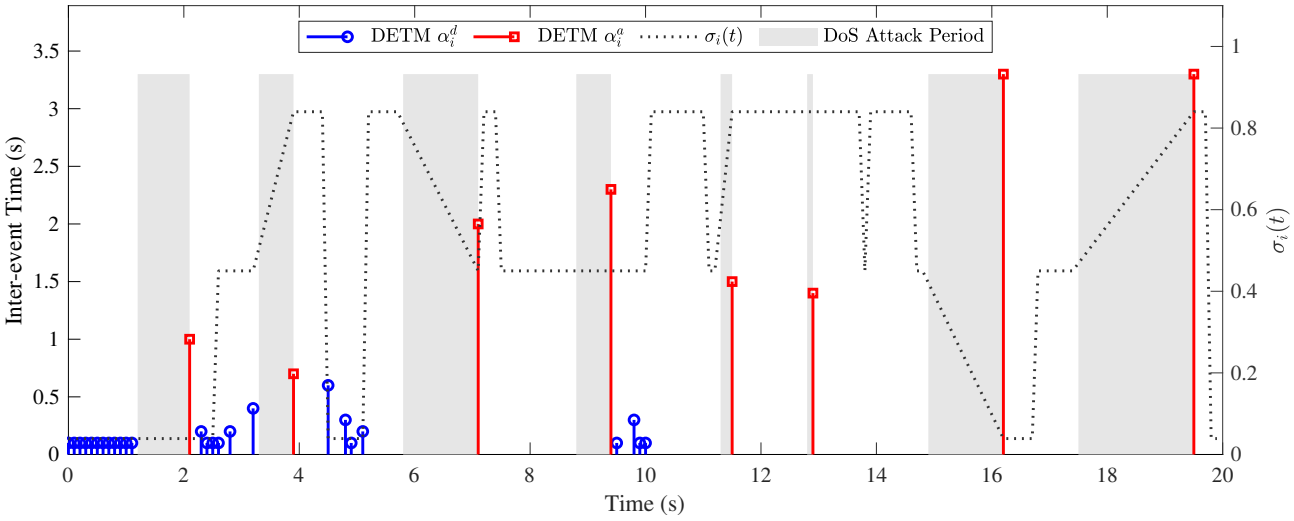


Figure 5. Inter-event intervals and adaptive threshold $\sigma_i(t)$ under DoS attacks in Example 1.

As demonstrated in Table 1, the proposed HETM dynamically adapts to varying network conditions. In Mode 1, the idle state, it yields an RBOR of 38.18% to facilitate rapid initial stabilization. Conversely, during Mode 3, the congested state, the RBOR drops to 5.48%. This autonomous adjustment effectively mitigates network loads and prevents severe channel congestion.

To quantitatively evaluate the overall communication efficiency and system convergence, the TPN and the integral of squared error (ISE) are adopted as the primary performance metrics.

Based on these metrics, Table 2 and Figure 6 compare the performance of the proposed HETM against existing event-triggered mechanisms under hybrid cyber-attacks. To ensure a fair comparison, all comparative simulations were conducted under the identical experimental conditions, including the same SMJNNs plant and cyber-attack scenarios. The results indicate that the proposed HETM achieves a more favorable trade-off between communication efficiency and control performance. Specifically, compared to the traditional DETMs presented by [40,41], the HETM significantly reduces the TPN to 34, alleviating the network burden. Furthermore, while the IETM proposed by [42] achieves a lower TPN of 17, it suffers from severe control performance degradation, yielding a high ISE of

5.2042. In contrast, the proposed HETM guarantees the lowest ISE value of 1.3531 and exhibits the smoothest transient state trajectories in Figure 6, confirming its effectiveness in co-optimizing resource utilization and system robustness.

Table 1. Comparison of communication performance across different operational modes in Example 1.

Mode	Status	α_i	TPN	N_{total}	RBOR	ARI (s)
1	Idle	0.90	21	55	38.18%	0.2619
2	Normal	0.50	9	72	12.50%	0.8000
3	Congested	0.20	4	73	5.48%	1.8250
Total	–	–	34	200	17.00%	0.5909

Note: α_i is the mode-dependent weighting parameter. TPN and N_{total} denote the transmitted packet number and total sampled packets, respectively. RBOR represents the relative bandwidth occupancy rate, and ARI indicates the average release interval.

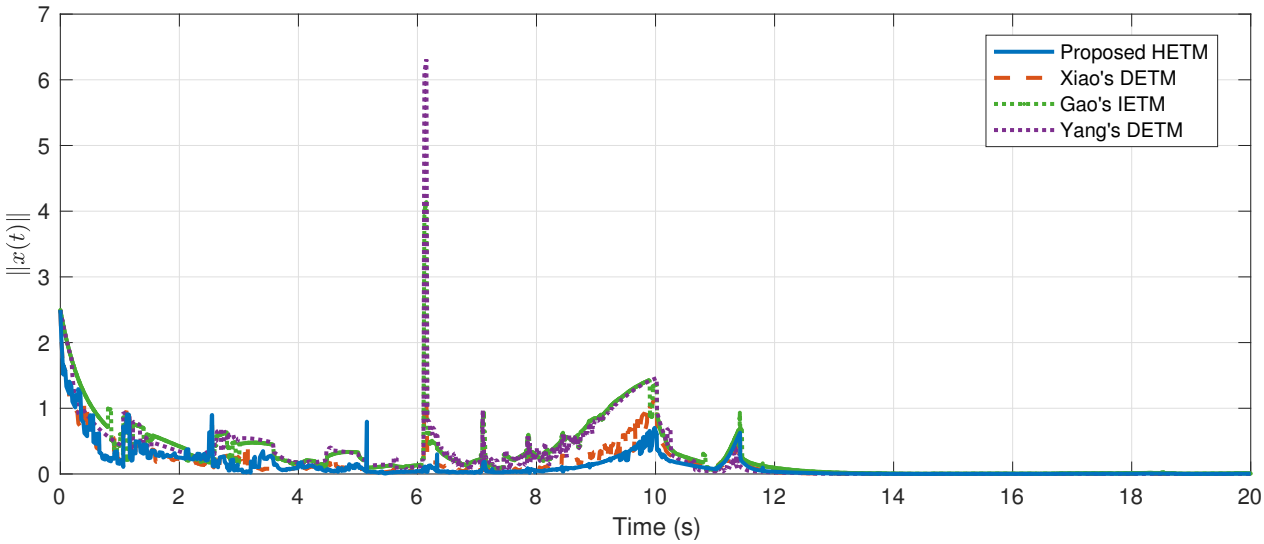


Figure 6. Trajectories of the system state norm $\|x(t)\|$ under different ETMs in Example 1.

Table 2. Comparison of communication and control performance across different ETMs in Example 1.

Mechanism	TPN	ARI (s)	ISE
Proposed HETM	34	0.5882	1.3531
DETM [40]	67	0.2985	1.6992
DETM [41]	61	0.3279	5.7125
IETM [42]	17	1.1765	5.2042

4.2. Example 2

Consider a typical artificial neural network consisting of n interconnected units [43]. Based on Kirchhoff's Current Law, the dynamical model of the k-th neuron is governed by

$$\begin{cases} \mathcal{E}_k \frac{\mathrm{d}x_k(t)}{\mathrm{d}t} = -\frac{x_k(t)}{\mathcal{T}_k(r_t)} + \sum_{j=1}^{n} \vartheta_{kj}^{(1)}(r_t) y_j(t) + \sum_{j=1}^{n} \vartheta_{kj}^{(2)}(r_t) y_j(t - d(t)), \ k = 1, 2, \ldots, n, \\ y_k(t) = g_k(x_k(t)), \end{cases} \tag{52}$$

where $x_k(t)$ and $y_k(t)$ correspond to the voltage state and nonlinear activation output of the k-th neuron, respectively; $\mathcal{E}_k$ is the capacitance parameter; and $\mathcal{T}_k(r_t)$ denotes the equivalent parallel resistance, which is given by

$$\frac{1}{\mathcal{T}_k(r_t)} = \frac{1}{\varrho_k} + \sum_{j=1}^{n} \frac{1}{\mathcal{T}_{kj}^{(1)}(r_t)} + \sum_{j=1}^{n} \frac{1}{\mathcal{T}_{kj}^{(2)}(r_t)}$$

where ϱ_k represents the inherent input resistance of the k-th operational amplifier, while $\mathcal{T}_{kj}^{(1)}(r_t)$ and $\mathcal{T}_{kj}^{(2)}(r_t)$ represent the instantaneous and delayed synaptic weights, which are defined based on the connection polarity as follows:

$$\vartheta_{kj}^{(l)}(r_t) = \begin{cases} +\frac{1}{\mathcal{T}_{kj}^{(l)}(r_t)}, & \text{if } \mathcal{T}_{kj}^{(l)}(r_t) \text{ is connected to } +y_j(t), \\ -\frac{1}{\mathcal{T}_{kj}^{(l)}(r_t)}, & \text{if } \mathcal{T}_{kj}^{(l)}(r_t) \text{ is connected to } -y_j(t). \end{cases} \quad (l = 1, 2)$$

By defining the state vector $x(t) = [x_1(t), x_2(t), \ldots, x_n(t)]^T$ and taking into account the time-varying transmission delay $d(t)$ over the open network as well as the control input $u(t)$, system (52) can be rewritten in the following matrix form.

$$E\dot{x}(t) = A(r_t)x(t) + G_1(r_t)g(x(t)) + G_2(r_t)g(x(t - d(t))) + B(r_t)u(t)$$

To implement the three-neuron network via an analog RC circuit, the capacitances are chosen as $\mathcal{E}_1 = \mathcal{E}_2 = 1$ F and $\mathcal{E}_3 = 0$ F, subject to the singular constraint $-2.5x_1(t) + 1.5x_2(t) - 5.0x_3(t) = 0$. For $i \in \{1, 2, 3\}$, the parameters of SMJNN (1) are given by

$$A_1 = \begin{bmatrix} -0.5 & 0 & 0 \\ 0 & -0.5 & 0 \\ -2.5 & 1.5 & -5.0 \end{bmatrix}, B_1 = \begin{bmatrix} 0.3 & 0.2 & 0.1 \\ 0.2 & 0.3 & 0.2 \\ 0.2 & 0.1 & -0.3 \end{bmatrix}, C_1 = \begin{bmatrix} 0.03 & 0.02 & -0.2 \\ 0.3 & 0.01 & -0.02 \\ 0.02 & 0.04 & 0.1 \end{bmatrix},$$

$$G_{11} = \begin{bmatrix} 1 + \frac{\pi}{4} & 0.1 & 0 \\ 0.1 & -0.3 & 0 \\ 0 & 0 & 0 \end{bmatrix}, G_{21} = \begin{bmatrix} 0.2 & -0.1 & 0.04 \\ -0.03 & 0.2 & 0.01 \\ 0.1 & 0.01 & 0.02 \end{bmatrix}, \begin{array}{l} \underline{L}_1 = \text{diag}\{0.1, 0.1, 0.05\}, \\ \overline{L}_1 = \text{diag}\{0.2, 0.3, 0.1\}, \end{array}$$

$$A_2 = \begin{bmatrix} -1.5 & 0 & 0 \\ 0 & -1.5 & 0 \\ -2.5 & 1.5 & -5.0 \end{bmatrix}, B_2 = \begin{bmatrix} -0.1 & 0.05 & 0.1 \\ 0.2 & 0.1 & 0.02 \\ 0.2 & 0.1 & -0.1 \end{bmatrix}, C_2 = \begin{bmatrix} 0.01 & -0.04 & 0.05 \\ 0.03 & -0.1 & 0.03 \\ 0.2 & 0.1 & -0.2 \end{bmatrix},$$

$$G_{12} = \begin{bmatrix} 1 & 1.5 & 0 \\ 1.5 & -1 & 0 \\ 0 & 0 & 0 \end{bmatrix}, G_{22} = \begin{bmatrix} -0.1 & 0.2 & 0.05 \\ 0.04 & 0.1 & -0.2 \\ 0.2 & 0.03 & -0.1 \end{bmatrix}, \begin{array}{l} \underline{L}_2 = 0, \\ \overline{L}_2 = \text{diag}\{0.8, 0.8, 0.8\}, \end{array}$$

$$A_3 = \begin{bmatrix} -1.0 & 0 & 0 \\ 0 & -1.0 & 0 \\ -2.5 & 1.5 & -5.0 \end{bmatrix}, B_3 = \begin{bmatrix} -0.2 & -0.1 & 0.3 \\ 0.2 & -0.1 & 0.2 \\ 0.2 & -0.3 & 0.1 \end{bmatrix}, C_3 = \begin{bmatrix} 0.01 & 0.03 & -0.01 \\ -0.2 & 0.05 & 0.02 \\ -0.1 & 0.03 & -0.05 \end{bmatrix},$$

$$G_{13} = \begin{bmatrix} -0.3 & 0.1 & 0 \\ 0.1 & 0.2 & 0 \\ 0 & 0 & 0 \end{bmatrix}, G_{23} = \begin{bmatrix} 0.1 & -0.01 & 0.2 \\ 0.02 & 0.1 & -0.03 \\ 0.04 & -0.1 & 0.05 \end{bmatrix}, \begin{array}{l} \underline{L}_3 = 0, \\ \overline{L}_3 = \text{diag}\{0.8, 0.8, 0.8\}, \end{array}$$

$$E = \begin{bmatrix} 1 & 0 & 0 \\ 0 & 1 & 0 \\ 0 & 0 & 0 \end{bmatrix}, \Pi = \begin{bmatrix} -1.7 & 0.8 & 0.9 \\ 0.5 & -0.9 & 0.4 \\ 1 & 0.8 & -1.8 \end{bmatrix}.$$

For the HETM, the mode-dependent triggering parameters are $\bar{\sigma}_i \in \{0.4, 0.6, 0.95\}$, $\underline{\sigma}_i \in \{0.01, 0.4, 0.6\}$, $\alpha_i \in \{0.9, 0.5, 0.2\}$, $\lambda_i \in \{0.4, 0.2, 0.1\}$, $\hat{\mu}_i \in \{0.5, 1.0, 1.5\}$, $\hat{\kappa}_i \in \{0.5, 1.0, 1.5\}$, $\psi_i \in \{1, 1.05, 1.1\}$, $\epsilon_{1i} = \epsilon_{2i} = 0.1$, $\chi_{i0} \in \{10^{-4}, 5 \times 10^{-4}, 10^{-3}\}$, $\gamma_1 = 0.4$, $\gamma_2 = 0.3$ and $\varpi_1 = \varpi_2 = 1.01$. Furthermore, $\bar{\beta} = 0.5$, $\mathbb{T}_{\min} = 1$ and $\mathbb{T}_{\max} = 2$

to represent an adverse network environment. The deception attack signal is defined as $f(y(t)) = [0.1y_1(t) + 0.1\tanh(y_1(t)), 0.1y_2(t) + 0.2\tanh(y_2(t)), 0.05y_3(t) + 0.05\tanh(y_3(t))]^T$. The activation function is $g(x_i(t)) = 0.4(|x_i(t) + 1| - |x_i(t) - 1|)$.

Solving the LMIs formulated in Theorem 1 yields the controller gains K_i and the weighting matrices Ω_i as follows:

$$K_1 = \begin{bmatrix} -0.4864 & -4.4474 & 0.2135 \\ 1.1848 & 4.0408 & -0.8615 \\ -1.5281 & -1.7510 & 0.6184 \end{bmatrix}, \Omega_1 = \begin{bmatrix} 3.8681 & -0.9650 & 6.3156 \\ -0.9650 & 0.5823 & -1.5260 \\ 6.3156 & -1.5260 & 13.1951 \end{bmatrix};$$

$$K_2 = \begin{bmatrix} 1.1994 & 2.2533 & -0.7476 \\ -1.8120 & -2.5343 & 0.4478 \\ 1.7891 & 2.6890 & -5.4003 \end{bmatrix}, \Omega_2 = \begin{bmatrix} 3.4255 & -1.3221 & 0.3232 \\ -1.3221 & 0.7603 & -0.0918 \\ 0.3232 & -0.0918 & 0.0534 \end{bmatrix};$$

$$K_3 = \begin{bmatrix} -0.1976 & -1.3446 & -0.7253 \\ -0.3222 & -0.5508 & -0.8907 \\ -0.3228 & 0.5189 & -0.0378 \end{bmatrix}, \Omega_3 = \begin{bmatrix} 0.4019 & 0.0399 & -0.0792 \\ 0.0399 & 0.0363 & -0.0616 \\ -0.0792 & -0.0616 & 0.1407 \end{bmatrix}.$$

Moreover, let $x(0) = [0.6, -0.6, 0.15]^T, h = 0.1$ s. Under hybrid cyber-attacks, the state trajectories of the analog RC network circuit are illustrated in Figure 7. Furthermore, Figure 8 plots the event release instants and inter-event intervals, demonstrating how the adaptive threshold $\sigma_i(t)$ dynamically adjusts in response to the DoS attack sequences. Finally, Table 3 details the transmission performance. The results verify that the proposed HETM adaptively alleviates network burden during congestion, achieving a low bandwidth occupancy of 16.50%.

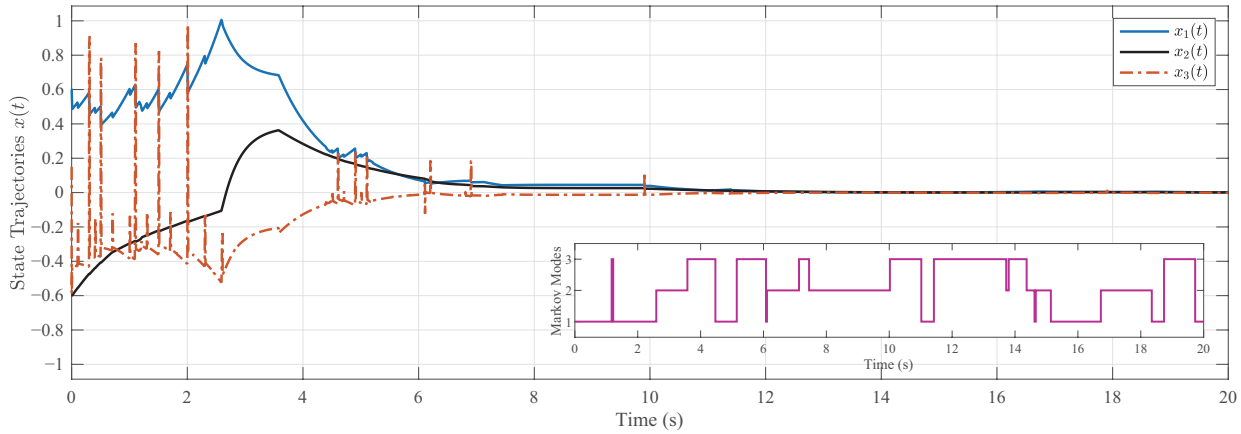


Figure 7. State responses of the RC network circuit in Example 2.

Table 3. Comparison of communication performance across different operational modes in Example 2.

Mode	Status	α_i	TPN	N_{total}	RBOR	ARI (s)
1	Idle	0.90	23	59	38.98%	0.2565
2	Normal	0.50	6	71	8.45%	1.1833
3	Congest	0.20	4	70	5.71%	1.7500
Total	–	–	33	200	16.50%	0.6061

Note: α_i is the mode-dependent weighting parameter. TPN and N_{total} denote the transmitted packet number and total sampled packets, respectively. RBOR represents the relative bandwidth occupancy rate, and ARI indicates the average release interval.

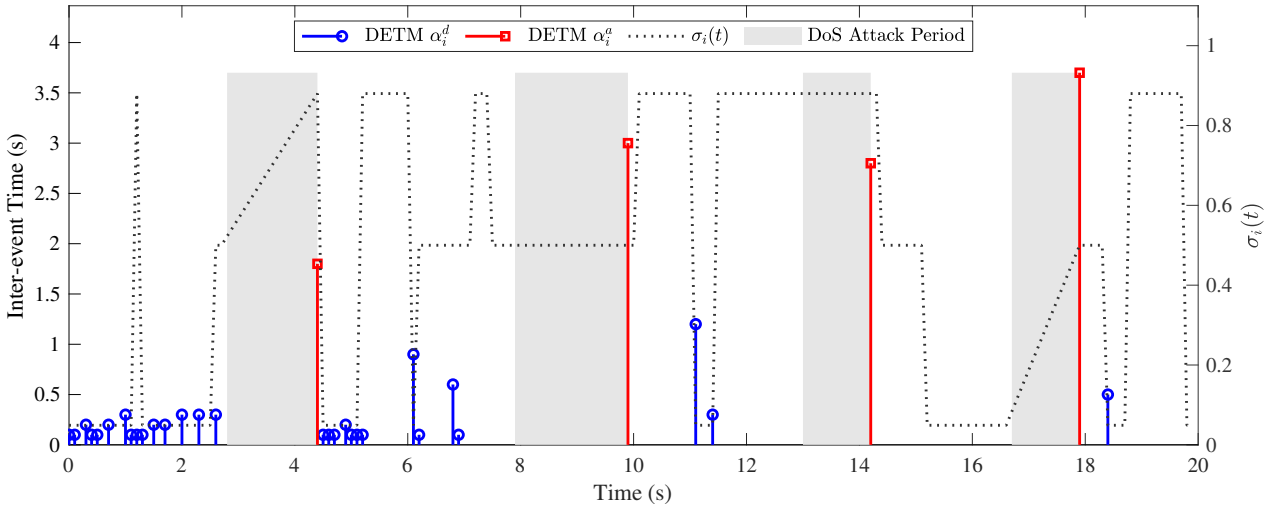


Figure 8. Inter-event intervals and adaptive threshold $\sigma_i(t)$ under DoS attacks in Example 2.

5. Conclusions

This paper has addressed the secure impulsive control problem for SMJNNs subject to hybrid DoS and deception attacks. To alleviate the network communication burden while ensuring system security, a novel mode-dependent HETM was proposed. Within this mechanism, the triggering thresholds are adaptively adjusted based on real-time bandwidth occupancy, Markovian modes, and the DoS attack status. Furthermore, a unified co-design framework integrating the proposed HETM and a mode-dependent impulsive controller was established to counteract concurrent cyber-threats. By constructing an appropriate LKF, effective sufficient conditions were derived to guarantee the admissibility of the closed-loop system. Finally, numerical and analog circuit simulations were provided to demonstrate the effectiveness of the proposed co-design approach.

Future research will focus on extending the proposed secure control framework to more general complex networked systems in practical applications.

Author Contributions: W.X. wrote the main manuscript text, conducted numerical simulation experiments and prepared all the figures. Y.Z. provided conceptualization and methodology. All authors have read and agreed to the published version of the manuscript.

Funding: This research received no external funding.

Data Availability Statement: The original contributions presented in this study are included in the article. Further inquiries can be directed to the corresponding author.

Conflicts of Interest: The authors declare no conflicts of interest.

Appendix A. The Proof of Equation (31)

Proof. This appendix provides the detailed derivation of the related impulsive parameter ϑ_i at the impulsive instants t_k^n. For simplicity of presentation, let $t_* \triangleq t_k^n$.

Driven by the impulsive control, the system state exhibits an instantaneous jump formulated as

$$\begin{aligned} x(t_*^+) =& x(t_*^-) + B_i K_i \tilde{y}(t_*^-) \\ =& x(t_*^-) + B_i K_i \mathscr{D}_D(t)[\beta(t) y(t_*^-) + \tilde{\beta}(t) f(y(t_*^-))] \\ =& x(t_*^-) + B_i K_i [\beta(t) C_i x(t_*^-) + \tilde{\beta}(t) f(C_i x(t_*^-))] \end{aligned} \tag{A1}$$

Denote $Z_i = E^T P_{1i} E \geq 0$. To guarantee the impulsive condition (31), we require $\mathbb{E}\{V_{11}((t_k^n)^+) - \vartheta_i V_{11}((t_k^n)^-)\} \leq 0$, thus

$$\mathbb{E}\{[\Gamma_{1i}x(t_*^-) + \Gamma_{2i}\tilde{f}]^T Z_i [\Gamma_{1i}x(t_*^-) + \Gamma_{2i}\tilde{f}] - \vartheta_i x^T(t_*^-) Z_i x(t_*^-)\} \leq 0 \tag{A2}$$

with $\Gamma_{1i} = I + \beta(t)B_iK_iC_i$, $\Gamma_{2i} = \tilde{\beta}(t)B_iK_i$, and $\tilde{f} = f(C_ix(t_*^-))$.

For notation brevity, let $\phi_k = [x^T(t_*^-), \tilde{f}]^T$. The inequality (A2) can be rewritten in a quadratic form.

$$\Theta_i^1 = \phi_k^T \begin{bmatrix} \Gamma_{1i}^T Z_i \Gamma_{1i} - \vartheta_i Z_i & \Gamma_{1i}^T Z_i \Gamma_{2i} \\ * & \Gamma_{2i}^T Z_i \Gamma_{2i} \end{bmatrix} \phi_k \leq 0 \tag{A3}$$

Also, the boundary condition in (28) can be rewritten as $\phi_k^T \Theta_i^2 \phi_k \leq 0$ with

$$\Theta_i^2 = \begin{bmatrix} 2C_i^T \underline{L}_1^T \Lambda_1 \overline{L}_1 C_i & -C_i^T (\underline{L}_1^T + \overline{L}_1^T)\Lambda_1 \\ * & 2\Lambda_1 \end{bmatrix} \tag{A4}$$

According to the S-procedure in Lemma 4, the condition $\Theta_i^1 \leq 0$ is guaranteed whenever $\Theta_i^2 \leq 0$, provided that there exists a scalar $\tau_{\text{imp}} \geq 0$ satisfying

$$\Theta_i^3 = \begin{bmatrix} \Gamma_{1i}^T Z_i \Gamma_{1i} - \vartheta_i Z_i & \Gamma_{1i}^T Z_i \Gamma_{2i} \\ * & \Gamma_{2i}^T Z_i \Gamma_{2i} \end{bmatrix} - \tau_{\text{imp}} \Theta_i^2 \leq 0 \tag{A5}$$

Since E is singular, Z_i is non-invertible, precluding the direct use of the standard Schur complement. To overcome this, a regularized matrix $\hat{Z}_i = Z_i + \epsilon I$ is defined to ensure invertibility, where ϵ is a sufficiently small positive scalar, and a relaxation matrix Q_{imp} is introduced to bound its inverse, yielding

$$\begin{bmatrix} \hat{Z}_i & I \\ I & Q_{\text{imp}} \end{bmatrix} \geq 0$$

To decouple the bilinear terms involving K_i, we define $N_i = B_iK_i$, $M_i = N_iC_i$, yielding

$$\Gamma_{1i} = (I + \beta(t)M_i), \quad \Gamma_{2i} = \tilde{\beta}(t)N_i$$

Finally, to guarantee the admissibility of the SMJNN in (12), the equality constraint $(I - EE^{\dagger})N_i = 0$ is imposed.

Applying the Schur complement in Lemma 3 to the linearized inequalities yields LMIs (15) and (16) in Theorem 1, which completes the proof. □

References

1. Guo, Y.; Wang, W.; Basin, M.V.; Shen, H. Asynchronous Filtering for Semi-Markov Jump Singular Systems With General Transition Rates via Dynamic Memory Event-Triggered Protocols. *IEEE Trans. Syst. Man Cybern. Syst.* **2026**, *56*, 5429–5442. [CrossRef]
2. He, K.; Xu, Q.; Sun, K.; Song, B. Event-triggered-based fault detection filter design for discrete-time networked singular systems. *Int. J. Syst. Sci.* **2026**, *57*, 401–413. [CrossRef]
3. Lewis, F.L. A survey of linear singular systems. *Circuits Syst. Signal Process.* **1986**, *5*, 3–36. [CrossRef]
4. Qiu, H.; Wang, H.; Pan, Y.; Cao, J.; Liu, H. Stability and L_∞-gain of positive fractional-order singular systems with time-varying delays. *IEEE Trans. Circuits Syst. II Exp. Briefs* **2023**, *70*, 3534–3538. [CrossRef]
5. Dehnavi, V.S.; Shafiee, M.; Mirshahi, M. Model-based fault-tolerant optimal control of fractional-order singular systems optimized via a novel data-driven approach. *Inf. Sci.* **2026**, *739*, 123175. [CrossRef]
6. RoshanaeeDeh, A.; Shafiee, M.; Atrianfar, H. Optimal control guaranteed H_∞ performance of uncertain 2-D singular systems under disturbances with uncertain actuator dynamics. *J. Frankl. Inst.* **2025**, *362*, 108150. [CrossRef]

7. Sun, C.; Li, R.; Cao, J.; Tu, Z. Stability and synchronization analysis for memristive neural networks with encryption and decryption of image on time scales. *Nonlinear Dyn.* **2025**, *114*, 16. [CrossRef]
8. Yu, S.; Shi, G.; Zhu, G.; Liu, Y.; Hu, S. Prescribed-Performance Control of Underactuated MSVs via a Neural Network-Based RISE Disturbance Observer. *IEEE Internet Things J.* **2026**, *Early access*. [CrossRef]
9. Xue, H.; Ge, X.; Zhang, Y.; Wang, Z.; Vong, S. Auxiliary matrix weighted functions approach and its application to delayed neural networks system. *J. Frankl. Inst.* **2026**, *363*, 108659. [CrossRef]
10. Zhang, X.; Chen, S.; Zhang, J.X. Adaptive sliding mode consensus control based on neural network for singular fractional order multi-agent systems. *Appl. Math. Comput.* **2022**, *434*, 127442. [CrossRef]
11. Wang, B.; Zhu, Q. The stabilization problem for a class of discrete-time semi-Markov jump singular systems. *Automatica* **2025**, *171*, 111960. [CrossRef]
12. Kao, Y.; Han, Y.; Zhu, Y.; Shu, Z. Stability analysis of delayed discrete singular piecewise homogeneous Markovian jump systems with unknown transition probabilities via sliding-mode approach. *IEEE Trans. Autom. Control* **2024**, *69*, 315–322. [CrossRef]
13. Tang, Y.; Zhou, X.; Li, P.; Cao, J.; Cheng, J. Sliding mode control for Markov jump singularly perturbed systems under piecewise homogeneous stochastic communication protocol. *IEEE Trans. Cybern.* **2024**, *54*, 4002–4013. [CrossRef] [PubMed]
14. Yin, Y.; Zhuang, G.; Xia, J.; Chen, G. Asynchronous H_∞ filtering for singular Markov jump neural networks with mode-dependent time-varying delays. *Neural Process. Lett.* **2022**, *54*, 5439–5456. [CrossRef]
15. Zhuang, T.; Yin, S.; Zhang, X.; Wang, J. Event-Triggered Impulsive Control for Switched Systems Under Aperiodic Denial-of-Service Attacks. *Mathematics* **2026**, *14*, 2365. [CrossRef]
16. Zhao, R.; Zuo, Z.; Tan, Y.; Wang, Y.; Zhang, W. Resilient control of networked switched systems subject to deception attack and DoS attack. *Automatica* **2024**, *169*, 111833. [CrossRef]
17. Tan, Y.; Yuan, X.; Yang, Y.; Wang, L.; Tan, Y. Event-Triggered Synchronization of T-S Fuzzy Neural Network with Quantized Encoding-Decoding Mechanism. *Mathematics* **2026**, *14*, 1081. [CrossRef]
18. Lai, G.; Xiang, S.; Liu, Z.; Huang, K.; Xiao, H.; Chen, C.L.P. Fixed-time adaptive fault-tolerant control for switched nonlinear systems with hysteresis inputs: Static and dynamic event-triggered schemes. *Nonlinear Dyn.* **2026**, *114*, 363. [CrossRef]
19. Meng, M.; Gan, Q.; Yang, J.; Xiang, K. Dynamic Event-Triggered Prescribed-Time Consensus of Second-Order Multi-Agent Systems Under Disconnected Time-Varying Topologies. *Mathematics* **2026**, *14*, 2688. [CrossRef]
20. Zeng, F.; Wang, Y.; Zhuang, G.; Chen, F. Dynamic-memory event-triggered-based controller design for singular stochastic semi-Markov jump systems against multiple cyber-attacks. *Nonlinear Dyn.* **2022**, *110*, 1559–1582. [CrossRef]
21. Shi, M.; Li, L.; Cao, J.; Hua, L.; Abdel-Aty, M. Stability analysis of inertial delayed neural network with delayed impulses via dynamic event-triggered impulsive control. *Neurocomputing* **2025**, *626*, 129573. [CrossRef]
22. Zhang, L.; Lu, J.; Jiang, B.; Ruan, Q.; Lou, J. Delay-dependent impulsive synchronization control for coupled dynamic networks under hybrid cyberattack. *Nonlinear Dyn.* **2025**, *113*, 11615–11630. [CrossRef]
23. Yang, G. State filtered disturbance rejection control. *Nonlinear Dyn.* **2025**, *113*, 6739–6755. [CrossRef]
24. Yang, G. Multilayer Neuroadaptive Reinforcement Learning of Disturbed Nonlinear Systems via Actor-Critic Mechanism. *IEEE Trans. Autom. Sci. Eng.* **2026**, *23*, 1372–1381. [CrossRef]
25. Pang, Y.; Zhuang, G.; Xia, J.; Xie, X.P. H_∞ Security Control for Singular Jump Systems With Actuator Faults and DoS Attacks Under Switching-Like Adaptive Trigger and Application to OCCP. *IEEE Trans. Autom. Sci. Eng.* **2025**, *22*, 7955–7966. [CrossRef]
26. Zhu, J.; Zhuang, G.; Chen, G.; Xie, X. Static output feedback quantized dissipative security control of singular hybrid systems subject to multiple cyber attacks: A dynamic-memory event-triggered strategy. *Commun. Nonlinear Sci. Numer. Simul.* **2024**, *128*, 107652. [CrossRef]
27. Bao, Y.; Zhao, D.; Sun, J.; Wen, G.; Yang, T. Resilient synchronization of neural networks under DoS attacks and communication delays via event-triggered impulsive control. *IEEE Trans. Syst. Man Cybern. Syst.* **2024**, *54*, 471–483. [CrossRef]
28. Zhuang, G.; Xia, J.; Feng, J.; Wang, Y.; Chen, G. Dynamic compensator design and H_∞ admissibilization for delayed singular jump systems via Moore-Penrose generalized inversion technique. *Nonlinear Anal. Hybrid Syst.* **2023**, *49*, 101361. [CrossRef]
29. Lin, H.; Zeng, H.; Zhang, X.; Wang, W. Stability analysis for delayed neural networks via a generalized reciprocally convex inequality. *IEEE Trans. Neural Netw. Learn. Syst.* **2023**, *34*, 7491–7499. [CrossRef] [PubMed]
30. Ghanim, D.A.; Bouzeffour, F.; Eddahbi, M. Markovian Dynamics Associated with d-Orthogonal Polynomials and Generalized Birth and Death Processes in Multiple-Life Insurance. *Mathematics* **2026**, *14*, 3257. [CrossRef]
31. Li, Q.; Zhang, K.; Abdurahman, A.; Wang, K.; Yang, J. HMM-based non-fragile dynamic event-triggered asynchronous H_∞ estimation for Markovian jumping neural networks with time-varying measurement delay. *Neurocomputing* **2026**, *663*, 132017. [CrossRef]
32. Liang, X.; Xia, J.; Shen, H. Sampled-data stabilization via novel looped-functional for fuzzy singular Markov jump system and its applications. *Inf. Sci.* **2026**, *728*, 122810. [CrossRef]
33. Tao, Y.; Wu, Z.; Huang, T.; Chakrabarti, P.; Ahn, C.K. Asynchronous event-triggered output-feedback control of singular Markov jump systems. *IEEE Trans. Cybern.* **2023**, *53*, 7342–7352. [CrossRef] [PubMed]

34. Wang, H.; Wang, Y.; Zhuang, G.; Xia, J. Finite-time event-based consensus control for singular semi-Markov jump multi-agent systems under deception attacks. *Int. J. Syst. Sci.* **2026**, *57*, 965–984. [CrossRef]
35. Ru, T.; Lin, H.; Cai, C. Secured consensus control for multi-agent systems under DoS attacks: Coding-decoding communication protocol. *Nonlinear Anal. Hybrid Syst.* **2024**, *52*, 101445. [CrossRef]
36. Zhou, K.; Zhang, Y.; Wei, M.; Ma, K. Dynamic event-triggered mean-square consensus of positive multi-agent systems via impulsive control under false data injection attacks. *J. Frankl. Inst.* **2024**, *361*, 106996. [CrossRef]
37. Zha, L.; Fang, J.; Liu, J.; Tian, E. Reliable control for hybrid-driven T-S fuzzy systems with actuator faults and probabilistic nonlinear perturbations. *J. Frankl. Inst.* **2017**, *354*, 3267–3288. [CrossRef]
38. Maharajan, C.; Raja, R.; Cao, J.; Rajchakit, G.; Tu, Z.; Alsaedi, A. LMI-based results on exponential stability of BAM-type neural networks with leakage and both time-varying delays: A non-fragile state estimation approach. *Appl. Math. Comput.* **2018**, *326*, 33–55. [CrossRef]
39. Zheng, Q.; Shi, W.; Wu, K.; Jiang, S. Robust H_∞ and guaranteed cost filtering for T-S fuzzy systems with multipath quantizations. *Int. J. Control Autom. Syst.* **2023**, *21*, 671–683. [CrossRef]
40. Xiao, S.; Ge, X.; Han, Q.L.; Zhang, Y. Dynamic Event-Triggered Platooning Control of Automated Vehicles Under Random Communication Topologies and Various Spacing Policies. *IEEE Trans. Cybern.* **2022**, *52*, 11477–11490. [CrossRef] [PubMed]
41. Yang, F.; Liu, J.; Guan, X. Distributed Fixed-Time Optimal Energy Management for Microgrids Based on a Dynamic Event-Triggered Mechanism. *IEEE Trans. Cybern.* **2024**, *11*, 2396–2407. [CrossRef]
42. Gao, H.; Jin, N.; Shi, K.; Wang, B.; Zhou, Y. Integral-based event-triggered reachable set estimation for networked switched fuzzy systems. *Asian J. Control* **2025**, *27*, 2558–2566. [CrossRef]
43. Li, W.; Xie, Z.; Wong, P.K.; Mei, X.; Zhao, J. Adaptive-Event-Trigger-Based Fuzzy Nonlinear Lateral Dynamic Control for Autonomous Electric Vehicles Under Insecure Communication Networks. *IEEE Trans. Ind. Electron.* **2021**, *68*, 2447–2459. [CrossRef]

Disclaimer/Publisher's Note: The statements, opinions and data contained in all publications are solely those of the individual author(s) and contributor(s) and not of MDPI and/or the editor(s). MDPI and/or the editor(s) disclaim responsibility for any injury to people or property resulting from any ideas, methods, instructions or products referred to in the content.